# Spatial transcriptomics reveals distinct lineage identities for major and minor vein initiation during maize leaf development

**Chiara Perico[1], Maricris Zaidem[1], Olga Sedelnikova[2], Samik Bhattacharya[3], Christian Korfhage[3] & Jane A. Langdale[1*]**

[1] Department of Biology, University of Oxford, South Parks Rd, Oxford, OX1 3RB, UK

[2] Syngenta Jealott's Hill International Research Centre, Bracknell, RG42 6EY, UK

[3] Resolve BioSciences GmbH, Alfred-Nobel-Straße 10, 40789 Monheim am Rhein, Germany

* Author for correspondence: jane.langdale@biology.ox.ac.uk

**PREPRINT SERVERS:** *BioRxiV* CC BY

**CLASSIFICATION:** Biological Sciences; Plant Biology

**KEY WORDS:** monocot, leaf, *Zea mays*, vein patterning, cell lineage, molecular cartography

## ABSTRACT

Leaves of flowering plants are characterised by diverse venation patterns. Patterning begins with the selection of vein-forming procambial initial cells from within the ground meristem of a developing leaf, a process which is considered to be auxin-dependent, and continues until veins are anatomically differentiated with functional xylem and phloem. At present, the mechanisms responsible for leaf venation patterning are primarily characterized in the model eudicot *Arabidopsis thaliana* which displays a reticulate venation network. However, evidence suggests that vein development may proceed via a different mechanism in monocot leaves where venation patterning is parallel. Here, we employed spatial transcriptomics to analyse the spatiotemporal localisation of a subset of auxin related genes and candidate regulators of vein patterning in maize leaves. We show how different combinations of auxin influx and efflux transporters are recruited during leaf and vein specification, and how major and minor vein ranks develop with distinct identities. The localisation of the procambial marker *PIN1a* and the spatial arrangement of procambial initial cells that give rise to major and minor vein ranks further suggests that vein spacing is pre-patterned across the medio-lateral leaf axis prior to accumulation of the PIN1a auxin transporter. In contrast, patterning in the adaxial-abaxial axis occurs progressively, with markers of xylem and phloem gradually becoming polarised as differentiation proceeds. Collectively our data suggest that both lineage- and position-based mechanisms underpin vein patterning in maize leaves.

## SIGNIFICANCE STATEMENT

During the development of multicellular organisms specialized cell-types differentiate from pluripotent stem cells, with cell identity acquired via lineage- or position-based mechanisms. In plants, most organs develop post-embryogenesis and as such developmental processes are influenced by the external environment. To adapt to different environmental contexts and yet still form recognizable organs, tissues and cell-types, position-based differentiation mechanisms are deployed in which cells adopt a certain fate depending on the activity of neighbouring cells. Such is the prevalence of position-based mechanisms in plant development that a role for lineage is rarely contemplated. Here we provide a rare example of lineage-based specification in maize where stem cells that give rise to different leaf vein types are inherently distinct at inception.

## INTRODUCTION

Within flowering plants distinct leaf venation patterns characterise the leaves of eudicotyledonous and monocotyledonous species, which display reticulate networks and parallel venation respectively (reviewed in (1)). The characteristics of parallel vein formation have been studied primarily in leaves of the monocot grass *Zea mays* (maize). As in all flowering plants, maize leaves emerge from the flanks of the shoot apical meristem (SAM) in a regular pattern. The SAM itself comprises two layers, an outer (epidermal) L1 layer and an inner L2 layer, both of which are recruited into new leaf primordia as they are formed (2). Leaves emerge sequentially on opposite sides of the SAM (alternate phyllotaxis) and at regular time intervals called plastochrons (P) (3) The incipient leaf, not yet distinguishable

anatomically but for which the position is already defined is referred to as P0, the youngest visible leaf primordium as P1, and older leaves with increasing plastochron numbers (4). Primordia inception is marked by an auxin maximum and by down-regulation of the homeobox gene *KNOTTED1* (*KN1*) which acts in the SAM to promote indeterminacy within both the central zone (CZ) of stem cells and the flanking peripheral zone (PZ) that gives rise to leaves. As primordia develop, proximo-distal (base-tip), medio-lateral (centre-margin) and adaxial-abaxial (upper-lower) leaf axes are established, each of which provides the spatial context in which veins develop (reviewed in (5)). Of particular importance is the establishment of a central layer of ground tissue in the adaxial-abaxial axis at P1, from within which all veins are subsequently initiated (6, 7). Parallel venation in maize leaves thus results from the specification of veins at regular intervals across the medio-lateral leaf axis, within a single layer of ground tissue in the adaxial-abaxial axis.

The maize leaf is characterised by several vein ranks which develop in a spatiotemporally regulated manner at successive plastochrons. Regardless of rank, development begins with the specification of a procambial initial cell (referred to as a pre-procambial cell in eudicots) within the central layer of the ground meristem. Once specified, this cell divides transversely to establish and extend the procambial strand in the proximo-distal leaf axis, and longitudinally/obliquely to form the procambial centre from which tissues of the vein differentiate in the medio-lateral and adaxial-abaxial leaf axes. Major veins, which include the mid- and lateral veins, develop acropetally (base-to-tip) along the proximo-distal axis with the midvein positioned in the middle of the developing primordium by P1 and lateral veins specified either side of it between P2 and P3. Minor veins, which include rank-1 and rank-2 intermediates, develop basipetally (tip-to-base) from P3 and are spaced regularly between the major veins such that each vein pair is separated by four cells (two mesophyll and two bundle sheath) across the medio-lateral axis (8–10). During the final stages of vein development, differentiation occurs in the adaxial-abaxial leaf axis, positioning xylem adaxially, phloem abaxially and sclerenchyma between the vein and epidermis. The final vein rank to form develops transversely, connecting the longitudinal veins across the medio-lateral leaf axis in a striate pattern.

Vein patterning mechanisms have been primarily studied in the model eudicot *Arabidopsis thaliana* where the auxin efflux carrier PIN1 is required for leaf initiation on the flanks of the SAM, specification of pre-procambial cells within the leaf primordium and directional extension of the procambial strands (11). In the SAM, the simultaneous action of *PIN1* and auxin influx carriers of the *AUX1/LAX* family generates the auxin maxima that determine the position of new leaves (12–14) and in the leaf *PIN1* activity induces the auxin activated transcription factors *MONOPTEROS* (*MP/ARF5*) and *ATHB8*, which commit cells from the ground meristem to pre-procambial and then procambial fate. A feedback loop between auxin transport, MP and ATHB8 then restricts the procambial strand to a couple of cell files in width (reviewed in (15)). The reticulate vein network results from the sequential specification of vein ranks with new veins developing towards pre-existing veins, which are used as positional landmarks towards which the auxin flux is directed (11, 16). The presence of parallel veins that are

precisely spaced across the medio-lateral leaf axis and a considerable expansion in the PIN and LAX transporter gene families (17) suggest that mechanisms underpinning vein patterning in monocots could be different from those found in *Arabidopsis*.

Recent genetic and transcriptome analyses have identified candidate regulators of venation patterns in monocot leaves. For example, a role for the *AINTEGUMENTA* (*ANT*) family in vein formation is supported by the finding that maize *ANT4* (18) is differentially expressed in median ground meristem (mGM) cells when compared to pre-mesophyll cells, and mutations in the *Setaria viridis AINTEGUMENTA1* (*ANT1*) gene lead to smaller leaves with distorted Kranz anatomy (19). Double mutations in *SCARECROW1* (*SCR1*) and its homeolog *SCR1h* condition narrower spaces between veins (20) and quadruple mutants with *NAKED ENDOSPERM1* (*NKD1*) and *NKD2* further enhance the spacing defect (21). In contrast, mutations in *SHORTROOT1* (*SHR1*) and its paralog *SHR2* disrupt the specification and/or subsequent development of veins (22–24), and mutations in *TOO MANY LATERALS* (*TML1*) form lateral veins in the position where the rank 1 intermediate veins that extend from blade to sheath normally develop (25). Whereas each of the genes mentioned thus far encode transcription factors, leaf venation defects have also been observed in mutants that perturb auxin biosynthesis, and transcriptome analyses have predicted a role for auxin transporters. For example, in *SPARSE INFLORESCENCE1* (*SPI1*) and *VANISHING TASSEL2* (*VT2*) mutants, reduced levels of auxin are associated with the formation of more intermediate veins in wider than normal leaves (26). Since neither pharmacological nor genetic approaches have disrupted the correlation between vein number and leaf width in monocots, any change of vein patterning accompanied by a change in leaf width is unlikely to result from directly disrupting the patterning mechanism (27). However, expression of the *AtPIN1* ortholog *ZmPIN1a* in all vein ranks from early stages of vein and leaf development (26) and a similar spatial expression pattern of the *LAX1* (note named *LAX2* in (18)) and *LAX2* (28) influx carriers at later stages of vein development, strongly suggest that auxin flux plays a role in vein patterning in the maize leaf. Although these observations are too fragmented to reveal any form of gene regulatory network, consistent expression profiles and mutant phenotypes of orthologs in different grass species (e.g. *TML1*, *SHR1, PIN1a/PIN1d*) suggest that core components of the mechanism underpinning parallel venation patterns in monocots have been identified.

Here we employed the Molecular Cartography spatial transcriptomics platform to investigate cellular relationships during early stages of maize leaf development. Spatial transcriptomics, a high-throughput quantitative *in situ* hybridization technology, allows single cell detection of transcripts combined with a visual interface to identify their localisation within a tissue (29–32). Focusing on candidate regulators of leaf initiation and vein patterning, we qualitatively and quantitatively defined spatial and temporal patterns of transcript accumulation across consecutive stages of development in maize shoot apices. These analyses revealed developmental patterns not previously detected by either morphological or cell lineage analyses, providing insight into the specification of procambial initial cells, the

establishment of procambial centres giving rise to different vein ranks, and the differentiation of tissues within each vein.

## RESULTS

*Spatial transcriptomics reliably reports transcript accumulation patterns in maize shoot apices*

We sought to generate a spatial expression atlas in maize shoot apices for genes in which an aberrant leaf venation phenotype has been described previously in either monocots or dicots (Table 1). This group of genes included auxin efflux and influx transporters such as *PIN* and LAX family members, auxin response transcription factors (ARFs) such as the *MP* co-orthologs *ARF4* and *ARF29*, plus candidate regulators of Kranz anatomy and vein patterning such as *TML1*, *SHR* and *SCR*. Hybridizations were carried out using transverse sections of wild-type B73 maize shoot apices, comprising the SAM (M) and the first five leaf primordia (P1 to P5) (Fig.1A-B). These stages allowed the spatial distribution of transcripts to be captured during the development of both major (midvein and laterals) and minor (rank 1 and rank 2 intermediate) veins (Fig. 1C). Data were collected across two experiments for a total of six sections. Calcofluor White (cell wall) and DAPI (nuclear DNA) staining allowed for automatic cell segmentation with CellPose 2.0 (33), (Fig.1B) and enabled qualitative and quantitative single-cell studies. A qualitative assessment showed consistency between spatial transcriptomics and traditional *in situ* hybridizations (Figure S1). For example, *KNOTTED 1* (*KN1)* transcripts were detected primarily in the L2 layer of the meristem with very low or no expression detected in the L1 layer (Fig. S1A), consistent with published reports (34–36). Similarly, *PIN1a* (Fig. S1B) and *TML1* (Fig. S1C) transcripts were detected as previously reported, that is in all veins at all stages of leaf development (*PIN1a*) (26) or in spaces between major veins where intermediate veins are developing (*TML1*) (25). For additional validation, we also carried out a traditional *in situ* hybridization with *LAX2*, an auxin influx transporter. With spatial transcriptomics, *LAX2* transcripts were detected in both major and minor veins (Fig. S1D), with higher levels detected in laterals (Fig. S1D, arrowheads) than intermediates (Fig. S1D, asterisks). These observations were consistent with results obtained by traditional *in situ* hybridization (Fig. S1E,F) (28). We thus concluded that spatial transcriptomics can reliably detect transcripts in transverse sections of maize shoot apices and that the single-cell information available following cell segmentation would enable a quantitative spatial expression atlas to be generated.

*Transcript clusters distinguish functional domains in the maize shoot apical meristem*

To investigate cellular relationships in the SAM, we segmented M-P1 stages and carried out qualitative and quantitative analyses of the candidate gene expression profiles within these tissues. Cluster analysis revealed five distinct cell identities across the M-P1 stage, which includes both the SAM and P1 primordium (Fig. 2A). To spatially visualise the clusters, two sections were analysed: the first (E1D2) cut across the shoot apex at the base of P1 (Fig. 2B-C) and the second (S1A1) cut across the shoot apex within the region of the P0 incipient leaf and included the tip of the P1 primordium (Fig. 2B, D). Images of both sections show that one cluster corresponds to the central zone of the SAM, with high

levels of *KN1* detected (yellow, Fig. 2B-C, Fig. S2). A second 'peripheral zone' cluster (green) is apparent either opposite a cluster corresponding to the developing P1 primordium (red, Fig. 2C) or completely encircling the central zone except for a few cells with leaf primordium identity (Fig. 2D, asterisks). Cells classified as dividing, due to the expression of genes encoding cyclins, primarily localise within the developing P1 primordium (blue, Fig. 2A-D). This observation is consistent with a rapid increase in cell number during early stages of leaf development. Finally, a handful of cells mark the boundary between the central zone of the meristem and the developing P1 primordium (magenta, Fig. 2A, C). Although the nature and function of these boundary cells in not clear, the other four clusters clearly demarcate regions of the SAM with distinct functions. Given that leaf primordia are initiated within the peripheral zone, we next sought to find traces of P0 identity in the peripheral zone opposite the tip of the P1 primordium (Fig. 2B). In *Brachypodium* and tomato, PIN1d generates the auxin maximum that determines the position of new leaves on the flanks of the SAM (37, 38). In our dataset, cells with the highest combined expression of both *PIN1d* (Fig. 2E) and *LAX5* (Fig. 2F) were positioned within the peripheral zone opposite the P1 primordium tip (Fig. 2G, Table S1). We therefore speculate that high levels of *LAX5* and *PIN1d* mark the position of P0 in the maize meristem.

*Leaf initiation and midvein formation are marked by distinct auxin transporters*

The role of auxin transporters in directing auxin towards sites of both leaf and midvein initiation is well documented in eudicots, with PIN1 playing a dominant role. To investigate whether specific auxin transporters are associated with leaf and/or midvein initiation in maize, we compared transcript accumulation profiles across the SAM and P1. Figure 3 shows hybridization of *PIN1d*, *PIN1a*, *LAX3* and *LAX5* to transverse sections of two regions of the SAM, along with a visual summary of our observations in a deduced longitudinal view. To verify our predicted P0 site, we first examined *KN1* transcript accumulation. Importantly, transcripts were detected in the inner layers of the shoot apical meristem (Fig. 3D-F) with near absence of accumulation in our predicted P0 region (Fig. 3E, dotted line). For the genes encoding efflux transporters, *PIN1d* transcripts were detected throughout the meristem and P1 (Fig. 3G-I), with the highest signal intensity at P0 (Fig. 3H). By contrast, *PIN1a* transcripts were localised to the central zone of the meristem and were restricted to the midvein position in the P1 primordium (Fig. 3J-L, asterisks). Notably, *PIN1a* transcript accumulation appeared to be contiguous between P0 and the centre of the meristem, suggesting the presence of an auxin conduit between P0 and the vasculature of the stem. Similar to the efflux carriers, the two influx transporters also showed distinct profiles. *LAX3* (Fig. 3M-O) and *LAX5* (Fig. 3P-R), which are co-orthologues of Arabidopsis *AUX1* and *LAX1* (17), were both detected in the peripheral zone of the meristem but not in the central zone or in the P1 primordium. However, *LAX5* transcripts were detected specifically in the newly forming P0 primordium (Fig. 3Q) whereas *LAX3* was detected both within and beyond the P0 region (Fig. 3N). Collectively these results reveal that *PIN1d* and *LAX5* mark the position of the P0 primordium within the peripheral zone of the SAM whereas *PIN1a* marks both the region in the SAM where the developing midvein will connect the new leaf to the vasculature of the stem, and the region in the P1 primordium where the midvein develops.

214

215 *A transcript cluster corresponding to major vein identity emerges at P2*

216 Whereas the midvein position is determined by P1, lateral veins continue to be specified during P2 and
217 thus to investigate cellular relationships at this later stage, we segmented P2 primordia and quantified
218 transcript levels in each cell. Cluster analyses revealed five cellular identities, which we labelled based
219 on the transcripts present and the spatial localisation within the primordium (Fig. 4A-C). Three of the
220 clusters identified the three main tissue types: epidermis, ground tissue and vascular tissue. Dividing
221 cells (as defined by expression of genes encoding cyclins) were present in all tissues types, although
222 at variable levels. Intriguingly, the profile of cells in the epidermal cluster varied slightly between
223 experiments. In one experiment there was a clear subdivision into two clusters (Fig. 4A-B, Fig. S2I-L):
224 an abaxial epidermal cluster (grey) and an adaxial epidermal plus leaf margin cluster (cyan). The
225 abaxial epidermis was characterized by high transcript levels of an epidermal marker (*MYB67*) and
226 several ARFs (*ARF16, ARF34*, *ARF23*, Fig. 4D), whereas the adaxial epidermis and leaf margin cluster
227 displayed high levels of *ANT4*, *PIN1d*, *LAX3* and *HB52* transcripts. This subdivision of the epidermal
228 tissue was not as marked in a second experiment, where an epidermal cluster was identified but there
229 was no clear subdivision between abaxial and adaxial/margin domains (Fig. S2G-H). Notably,
230 differences between experiments were also observed in overall *PIN1d*, *ARF16* and *ARF34* levels (Fig.
231 S3), suggesting that the detection of these transcripts may be more sensitive to subtle changes and
232 variations between experiments, or to the precise cutting plane of the sections or developmental stage
233 of the plant. In both experiments, cells in the ground tissue predominantly accumulated *ARF4* (*MP*),
234 *ANT4* and *LAX1* transcripts, as well as low levels of *RVN1*, *SCR1/SCR1h* and *TML1* (Fig. 4D).

235

236 Unlike the epidermis and ground tissue, which are derived from the SAM and are present at P0,
237 procambial initial cells that give rise to the leaf veins have to be specified from within the ground tissue
238 at successive stages of primordium development. Our data reveal that a cell cluster with vascular
239 identity emerges at P2 (orange, Fig. 4B-C) and that it includes both the midvein (Fig. 4C, arrowhead)
240 and lateral veins (Fig. 4C, asterisks). The cluster is characterized by high levels of *PIN1a*, *SHR1*,
241 *SHR2*, and *ANT4* transcripts and, to a lesser extent, *LAX1* and *LAX2*. Notably, the distance between
242 veins identified by this cluster is consistently four to five cells (Fig. 4C, bracket), which suggests that
243 venation patterns and the distance between veins are specified by P2. Also of note is that the midvein
244 and lateral veins form a single cluster despite representing two distinct vein ranks and developing at
245 different timepoints (Fig. 4C). Collectively, these results show that by P2 the maize leaf primordium
246 can be broadly subdivided into three major tissue types: ground tissue, epidermis and vasculature, with
247 vascular identity marked by the accumulation of *PIN1a*, *SHR1*, *SHR2* and *ANT4* transcripts.

248

249 *TML1 marks a distinct intermediate vein cluster at P3 and P4*

250 Given that all major veins can be identified by a specific transcript cluster at P2, we next investigated
251 whether minor vein ranks can be identified by the same or a different gene set. For this purpose, cluster
252 analysis was carried out with data from P3 and P4 primordia, to capture the development of rank-1

253 intermediate veins. Analysis of P3 and P4 primordia identified six and seven clusters respectively (Fig.
254 5A-D). In the context of the epidermis, as for P2, discrepancies were seen between experiments in
255 terms of whether the epidermis was divided into distinct zones: one cluster associated with the abaxial
256 epidermis and another with both the adaxial epidermis and the leaf margin (Fig. 4A,B; Fig. 5A,B,E,F;
257 Fig S2M-R – grey and cyan respectively). In both experiments, however, the epidermal cluster was
258 distinct from the ground tissue, which again was similar to that seen at P2 with *PIN1a*, *LAX1*, *RVN1*,
259 *ANT4*, *HB52*, *ARF4*, *ARF16* and *ARF34* transcripts detected (Fig. 4D, Fig. 5C,D). The striking
260 difference between clusters identified at P2 versus those identified at later stages was that two distinct
261 vascular clusters were evident at P3 and P4.
262
263 The spatial localisation of the two vascular clusters and the spacing between them within the P3 and
264 P4 primordia suggest that they represent distinct lateral (Fig. 5G,H - orange) and intermediate (Fig.
265 5G,H - magenta) vein identities. Both clusters share a common set of transcripts which include *PIN1a*,
266 *LAX1*, *ANT4*, *PIN1d*, *HB52*, *ARF16* and *ARF24*. However, the intermediate vein cluster is distinguished
267 by high levels of *TML1* transcript (Fig. 5C,D), which is consistent with the observation that the *tml1*
268 mutation in maize specifically perturbs the development of rank-1 intermediate veins. The intermediate
269 vein cluster also displays lower levels of *SHR1* and *SHR*2 transcripts than the lateral vein cluster (Fig.
270 5C,D). In conclusion, clustering of cells from stage P3 and P4 highlighted similarities and differences
271 in the development of different vein ranks. Both lateral and rank-1 intermediate veins accumulate a
272 similar set of auxin transporters and procambial markers, such as *PIN1a*, *LAX1*, *ANT4* and *HB52*.
273 However, the clear difference between the lateral and rank-1 intermediate vein clusters, and the
274 specific accumulation of *TML1* transcripts in the intermediate cluster, suggest that vein ranks are
275 transcriptionally distinct after just a few divisions of the procambial initial.
276
277 *Vein formation across the medio-lateral leaf axis reveals a temporal hierarchy of PIN1a, SHR1 and*
278 *LAX2 accumulation during early procambium development*
279 To determine the extent to which the spatial regulation of genes associated with vein formation is
280 accompanied by temporal regulation, we analysed the distribution of transcripts across the shoot apex.
281 For this analysis we focused on genes that are shared between lateral and intermediate veins clusters,
282 such as *PIN1a*, *SHR1*, *SHR2* and *ANT4,* in order to dissect events during the first few divisions of the
283 procambial initial. We discovered that *PIN1a* was the earliest and most persistent marker of vein
284 development, being detected at all stages of development from M-P1 to P5 (Fig. 6A). In M-P1, *PIN1a*
285 transcripts marked both the position of the developing midvein (Fig. 6B, white ellipse, “m”) and the
286 central zone of the meristem, suggesting a role in connecting the newly developing midvein with the
287 vasculature of the stem. From P2 onwards, transcripts were detected in all vein ranks of all leaf
288 primordia, i.e. the midvein (Fig. 6C-D, white ellipse) laterals (Fig. 6D, empty arrowheads) and
289 intermediates (Fig. 6D, filled arrowheads). Notably, *PIN1a* transcripts were detected before and after
290 procambial centres became anatomically distinguishable from the surrounding ground tissue, with
291 other procambial and vascular markers following the appearance of *PIN1a*. For example, we detected

292 transcripts of the GRAS transcription factor *SHR1* (Fig. 6E) at the same sites as *PIN1a*, but at a slightly
293 later stage of development. These observations revealed not only that the expression of *SHR1* occurs
294 after that of *PIN1a*, but also that the development of veins across the medio-lateral axis follows a
295 specific dynamic: veins closer to the midrib express *SHR1* earlier than those closer to the leaf margin.
296 In a similar manner, we observed that *LAX2* transcripts accumulated at least one plastochron later than
297 *SHR1* (Fig. 6F). Together our data suggest that PIN1a is the earliest leaf procambial marker at the
298 developmental stages considered in this study and that other procambial markers follow in a specific
299 temporal hierarchy.
300
301 *Vascular markers become polarized in the adaxial-abaxial axis at late stages of vein development*
302 Having observed that venation markers are sequentially expressed during procambium initiation, we
303 next investigated whether localisation could also vary between early and late stages of vein
304 development. We took into consideration two vein ranks, the midvein and lateral veins, for which a
305 trajectory from early specification (M-P1 and P2 stage) to phloem and xylem differentiation (P3 to P5)
306 could be traced across the developmental stages in our study. Several markers for which transcripts
307 are localised in all vein ranks were analyzed. A representative example is provided in Figure 7A, where
308 *PIN1a* (red), *HB52* (yellow) and *LAX2* (blue) transcripts are superimposed, and all transcripts are
309 detected in all vein ranks and at all leaf developmental stages. Regardless of vein rank, at stages prior
310 to differentiation of phloem or xylem, all three markers were detected throughout the procambial centre
311 (Fig. 7B). Once phloem and xylem were differentiated, however, *PIN1a*, *HB52* and *LAX2* transcripts
312 were polarly localized (Fig. 7C,E). In both the mid- (Fig. 7C) and lateral (Fig. 7E) veins, *PIN1a*
313 transcripts were detected on the adaxial side, *HB52* transcripts towards the phloem on the abaxial side,
314 and *LAX2* juxtaposed between the two. Collectively, our data suggest that vascular-associated genes
315 are tightly regulated temporally and spatially, both within and between different vein ranks, with
316 changes in spatial localisation marking transitions between the specification of procambial initial cells,
317 the development and extension of procambial strands, and differentiation of tissues within the vein.
318
319 **DISCUSSION**
320 Here we have used spatial transcriptomics and a set of marker genes associated with auxin transport
321 and vein patterning to investigate cellular relationships during leaf specification and vein formation in
322 maize shoot apices (Fig. 1). On leaf initation, we reveal that it is possible to identify the region
323 corresponding to incipient P0 leaves within the peripheral zone of the SAM, based on high density of
324 *PIN1d* and *LAX5* transcripts (Fig. 2). *PIN1a* transcripts connect the site of the incipient leaf with the
325 central zone of the meristem, likely connecting the new leaf with the vasculature of the stem and
326 determining the position of the midvein at P1 (Fig. 3). From P2 to P4, the specification of both major
327 (midvein and laterals) and minor (intermediate) vein ranks can be traced, with intermediate veins
328 characterized by the presence of the transcription factor *TML1* (Fig. 4, 5). Strikingly, the localisation of
329 the procambial marker *PIN1a* and the spatial position of major and minor vein clusters suggest that
330 vein spacing could be pre-patterned prior to *PIN1a* accumulation. Once *PIN1a* accumulation (and

presumably auxin flux along the proximo-distal leaf axis) is initiated, a spatiotemporal hierarchy is triggered in which vein markers accumulate in a sequential manner that is position-dependent across the medio-lateral leaf axis (Fig. 6). During the final stages of vein development, in which phloem and xylem are differentiated, vascular markers become spatially restricted in the adaxial-abaxial leaf axis (Fig. 7). Collectively these data suggest progressive restriction of gene expression in all three leaf axes as veins are specified, initiated, extended and then differentiated.

The importance of understanding cell lineage relationships during development has long been recognised, not least to distinguish mechanisms in which cell fate is inherently specified in descendents following mitosis, from those in which fate specification relies on positional information from neighbouring cells (reviewed in (39)). In maize, many aspects of leaf development have been elucidated by exploiting genetic mosaics, including the presence of distinct central and marginal lineages in the medio-lateral leaf axis (40, 41) and the presence of a lineage in the centre of the adaxial-abaxial axis from which all veins are derived (7). With the advent of single cell sequencing, and now spatial transcriptomics, discussions of lineage relationships have altered, with UMAPs and associated clustering approaches identifying cells with shared fates, regardless of whether that fate is determined by lineage-based or positional mechanisms (32, 42–44). Importantly, combining information from both approaches allows classical lineage distinctions to be associated with specific gene expression profiles and also facilitates more refinement of cellular relationships during later stages of development. For example, we identified transcriptionally distinct populations of cells in the peripheral zone of the SAM that will give rise to the P0 primordium, and identified two distinct populations of vein-forming procambial cells in the central ground meristem layer of P3 and P4 leaf primordia. Notably, some of the markers that defined developing procambial lineages, such as *PIN1a*, *TML1* and *HB52*, could be detected in a dispersed pattern prior to vein specification. For example, *TML1* transcripts were detected at P2, prior to intermediate vein specification, but accumulation patterns were not restricted to the central ground meristem layer. By contrast, *TML1* transcripts could only be detected in procambial cells that were dividing to form intermediate veins at P3. The identification of transcriptionally distinct cell populations within any particular cell lineage (*sensu stricto*) can thus inform when cell fate is specified by positional information.

In the context of vein patterning, cellular relationships identified through transcript profiles have revealed distinctions that have not been made previously by either cell lineage or histological analyses. The set of genes used in this study distinguished two separate cell clusters between stages P2 and P4, corresponding to major (midvein and lateral) and intermediate veins (Figs. 4, 5). No substantial differences were detected between midvein and lateral vein clusters, which were grouped together from P2 onwards. This observation could reflect the fact that our dataset does not include genes which are specific for either midvein or lateral vein identity. Alternatively, it suggests that the midvein and lateral veins are not intrinsically different, a suggestion supported by the phenotype of midribless mutants (45, 46). By contrast, minor veins are transcriptionally distinct from major veins once

370 procambium is specified, as evidenced by transcript localisation profiles and the phenotype of loss of
371 function *TML1* mutants (25). Although both minor and major veins are specified *de novo* from the
372 middle layer of the ground meristem, this observation suggests that procambial initials are inherently
373 distinct. This hypothesis is supported by the observation that intermediate veins start to be specified
374 near the midvein during P3, when growth in the medio-lateral axis is ongoing and lateral veins are still
375 being specified near the leaf margin (Fig. 5 G-H, orange). This leads to a gradient in the medio-lateral
376 axis, with veins closer to the midrib being more developed than those closer to the leaf margin (10). If
377 major and minor vein lineages were not inherently distinct, intermediate veins close to the midrib would
378 be of similar size to lateral veins close to the leaf margin but they are not. These findings suggest that
379 procambial initial cells that give rise to major and minor vein ranks in the maize leaf are distinct at
380 inception.
381
382 In the model eudicot *Arabidopsis thaliana,* auxin fluxes have been associated with vein patterning, with
383 pre-existing vasculature used as a positional landmark towards which auxin flows and new
384 procambium is initiated (11, 16). In contrast, the localisation of transcripts encoding auxin transporters
385 in maize suggests that auxin fluxes associated with procambial initiation are pre-patterned. Specifically,
386 *PIN1a* transcripts are first detected in individual procambial initial cells that are already spaced
387 appropriately across the medio-lateral axis. As such, *PIN1a* activity is not necessary to determine which
388 cells in the ground tissue will commit to procambial fate. Notably, the DR5 transcriptional reporter is
389 detected along the leaf margin in maize leaves, indicating that an auxin maximum is present at the
390 margin (26, 47). Given that PIN1a does not overlap with the DR5 signal at the margin of P0 to P5
391 primordia (26), auxin flux from the margin is unlikely to be inducing procambial initial cell specification
392 or procambial strand extension. Instead, an unidentified factor must be inducing PIN1a accumulation
393 in the subset of regularly spaced ground tissue cells that become procambial initial cells. Once *PIN1a*
394 is activated, other auxin transporters and vascular markers are detected in developing veins but
395 temporal and/or spatial patterns of transcript accumulation again suggest progressive restriction of
396 activity. For example, maize abaxial and adaxial markers *ARF3a* (*AUXIN RESPONSE FACTOR 3a*)
397 and *RLD1* (*ROLLED LEAF1*) are localised throughout the adaxial (RLD1) or abaxial (ARF3a) leaf
398 domains between P0 and P3, but by P4 they are primarily restricted to the vasculature and are
399 associated with differentiated xylem (*RLD1*) and phloem (*ARF3a*) (47). Together, these findings
400 suggest that the position of procambial initials in the medio-lateral axis of the maize leaf is pre-patterned
401 prior to auxin flux through the procambial strand, and that the patterning of differentiated tissues within
402 each vein is similarly pre-patterned in the adaxial-abaxial leaf axis.
403
404 The role of auxin in both leaf initation and vein patterning has been acknowledged for some time (1,
405 48) but the spatial transcriptomes reported here reveal new insights. In *Arabidopsis thaliana*, *PIN1* acts
406 as a master regulator of both leaf positioning and vein specification (11, 49, 50). In non-Brassicaceae,
407 however, the expansion of the PIN1 family and the emergence of a sister clade (SoPIN1/PIN1d)
408 enabled sub-functionalisation (17, 37, 38, 51). Our analysis reveals that positioning of the P0

409 primordium in maize is associated with combined accumulation of transcripts encoding the auxin efflux
410 and influx carriers *PIN1d* and *LAX5* (Fig. 3), whereas the specification of procambium is associated
411 with the accumulation of *PIN1a*, *PIN1d* and *LAX1*, with *LAX2* likely being the dominant influx carrier
412 later in vein development. Our results are consistent with previous findings where combined expression
413 of *PIN1a*, *PIN1d* and *LAX1* (note *LAX2* in (18)) was detected from procambial initial cell selection
414 through to later stages of procambium development ((18)). Detection of *PIN1d* but not *PIN1a* at the
415 site of the P0 primordium suggests a functional subdivision within the maize PIN1 family as seen in
416 tomato and *Brachypodium* (37, 50), with *PIN1d* (*SoPIN*) regulating phyllotaxy and *PIN1a* tracing the
417 midvein and its connection to the subtending vasculature (Fig. 3) (47). We further speculate that *LAX5*,
418 co-ortholog with *LAX3* of *Arabidopsis AUX1/LAX1*, supports the role of *PIN1d* in generating an auxin
419 maximum in the L1 of the SAM, whereas *LAX2* acts with *PIN1a* to extend procambial strands in the
420 proximo-distal leaf axis. Together, these findings suggest a subdivision of roles within both the *PIN1*
421 and *LAX* gene families that allows different combinations of auxin influx and efflux transporters to be
422 recruited in different developmental contexts.
423

424 **CONCLUSIONS**

425 This study used spatial transcriptomics to identify populations of cells with shared identity, and to
426 elucidate how those populations diverged during the course of leaf primordium development in maize.
427 Regardless of whether they arise as the result of positional or lineage-based cues, cell fates can be
428 associated with the spatial co-localisation of transcripts within a tissue. As such, we propose that major
429 and minor vein ranks in the maize leaf have distinct identities at inception from the ground meristem.
430 We further propose that veins in the maize leaf are pre-patterned in all three leaf axes, with auxin
431 triggering downstream specification events through finely tuned spatio-temporal accumulation of influx
432 and efflux transporters.
433

434 **METHODS**

435 *Plant growth conditions*

436 Wild-type B73 seeds were germinated and grown in an environment-controlled chamber with a 16 h/8
437 h day/night cycle, temperature 28°C/20°C, 50 % humidity and light intensity of 300 $\mu mol \cdot m^{-2} \cdot s^{-1}$. Seeds
438 were germinated in medium vermiculite and seedlings were harvested ten days after sowing.
439

440 *Tissue fixation and preparation for traditional in situ hybridization*

441 Traditional *in situ* hybridization was carried out using wax-embedded wild-type B73 maize shoot apices
442 as previously described (24) with a 268 bp digoxygenin (DIG)-RNA labelled probe complementary to
443 the 3'UTR sequence of the *LAX2* gene (starting at 126 bp downstream of the stop codon).
444

*Molecular Cartography probe design*

Probes were designed using Resolve BioSciences' proprietary design algorithm and gene annotations from the *Zea Mays* RefGen V4. The final set of probes was selected as outlined in (29).

*Tissue fixation and preparation for Molecular Cartography*

Shoot apices were cut just below and 0.5 cm above the shoot apical meristem and the resulting tissue was fixed in 4% ice-cold paraformaldehyde (PFA) under vacuum, until complete sinking of the samples. The tissue was then embedded in paraffin following the user guide for sample preparation from Resolve BioSciences. Samples were then dehydrated, cleared and wax infiltrated with Paraplast Plus. The clearing and wax infiltration steps were either carried out manually (samples E1B2, E1D2, S1B1 or S1B2) or using a TissueTek VIP processor (samples S1A1, S1A2). Wax-infiltrated samples were embedded in blocks of Paraplast Plus using a TissueTek TEC wax-embedding centre. A total of six 10 µm-thick transverse sections were cut with a microtome and baked onto a Molecular Cartography-compatible coverslip at 37°C overnight to allow for sample attachment. Sections underwent deparaffinization, permeabilization and refixation according to Resolve BioSciences' user guide. Samples were mounted in SlowFade Diamond Antifade and shipped to Resolve Biosciences for Molecular Cartography analysis.

At Resolve BioSciences, sections were washed twice in 1 × phosphate buffered saline (PBS) for 2 min, followed by 1 min washing in 50 % and 70 % ethanol at room temperature. Ethanol was removed by aspiration and DST1™ buffer was added, followed by tissue priming for 30 min at 37 °C and by a 48 h hybridization using probes specific for the target genes. Samples were washed to remove excess probes and fluorescently tagged in a two-step colour development process. Fluorescent signals were removed after imaging in a decolourization step. Colourization, imaging, and decolourization were iterated for multiple cycles to generate a unique combinatorial code for each target gene. Samples were imaged by Resolve BioSciences as described in (29). Two independent experiments were carried out – the first with sections E1B2 and E1D2 and the second with samples S1A1, S1A2, S1B1 and S1B2.

*Image pre-processing and cell segmentation*

Cell segmentation was carried out using CellPose 2.0 (33), starting from high resolution images of Calcofluor and DAPI-stained sections. A pre-processing step was carried out to facilitate cell segmentation. Firstly, DAPI and Calcofluor images were overlaid in ImageJ: the co-existence of cell wall and nuclear staining allows for more accurate segmentation with CellPose 2.0. Subsequently, different stages of leaf development were cropped and isolated from the overlay image: this allows for faster computational speed during the segmentation step, and for a more accurate estimate of the average cell diameter, which varies greatly between leaf primordia. The images of isolated leaf primordia were imported into CellPose 2.0, and the Calcofluor and DAPI channels brightness and contrast were adjusted as required. The "cyto2" model was used to predict the cell boundaries in M-P1

484 and P2 primordia, whereas the “TN2” model was used to predict cell boundaries in P3, P4 and P5
485 primordia. All segmentations were then manually corrected, and the resulting masks were used to train
486 a custom model. All subsequent primordia underwent segmentation using the custom models thus
487 obtained and corrected manually when required. Segmented cells were exported as PNG masks and
488 converted to ROIs using the ImageJ plugin “Labels to ROIs”. ROIs were then used to visualize single-
489 cell gene expression using the proprietary Molecular Cartography plugin from Resolve Biosciences.
490
491 *Data analysis*
492 All data analyses and plots were carried out with R Studio and the Molecular Cartography ImageJ
493 plugin proprietary of Resolve Biosciences. Raw single-cell data was extracted from the spatial images
494 using the ImageJ plugin from Resolve BioSciences. The raw data was then analysed with the R
495 package Seurat to carry out all data analyses and clustering and generate all plots. Briefly, for each
496 developmental stage, the raw data was first normalised using a standard log-normalization
497 (NormalizeData), then subject to principal component dimensionality reduction (RunPCA) using the
498 default parameters. The dimensionality was further reduced by running the Uniform Manifold
499 Approximation and Projection (UMAP) dimensionality reduction to generate the clusters. Correlation
500 plots were generated to evaluate linear relationships between genes across experimental repeats.
501
502 *Data access*
503 All raw data, Calcofluor White and DAPI images and cell segmentations are deposited on Zenodo.
504
505 **LIST OF SUPPLEMENTARY MATERIAL**
506 **Table S1**. Gene expression in P0 cells identified from the ‘peripheral zone’ cluster.
507 **Figure S1**. Validation of spatial transcriptomics for localization of transcripts in maize shoot apices.
508 **Figure S2**. Visual representation of clusters at all stages of leaf development.
509 **Figure S3**. Correlation analysis of the Molecular Cartography datasets.
510
511 **AUTHOR CONTRIBUTIONS**
512 CP and JAL conceived and designed the experiments, MZ and CP wrote the code and performed the
513 cluster analysis, OS carried out the traditional *in situ* hybridization experiments, SB carried out the
514 spatial transcriptomics hybridizations under the supervision of CK, CP performed all the sample
515 preparation and data analysis; CP and JAL wrote the first draft of the manuscript and all authors
516 contributed to the final version.
517
518 **ACKNOWLEDGEMENTS**
519 The authors thank all members of the Langdale lab for constructive discussions of the results and data
520 analysis, and feedback on the manuscript. We also thank Thomas Hughes for helping with the sample
521 preparation, and Tina Schreier, Hilde Nelissen, Jessica Joossens and Denia Herwegh for feedback on
522 the manuscript.

## COMPETING INTERESTS

SB and CK are employees of Resolve Biosciences which is the proprietor of Molecular Cartography technology. All other authors declare no competing interests.

## FUNDING

This research was funded by the Bill and Melinda Gates Foundation $C_4$ Rice grant awarded to the University of Oxford 2019-2024 (INV-002970).

## REFERENCES


1. C. Perico, S. Tan, J. A. Langdale, Developmental regulation of leaf venation patterns: monocot versus eudicots and the role of auxin. *New Phytologist* **234**, 783–803 (2022).
2. R. S. Poethig, I. M. Sussex, The cellular parameters of leaf development in tobacco: a clonal analysis. *Planta* **165**, 170–184 (1985).
3. R. O. Erickson, F. J. Michelini, The plastochron index. *Am J Bot* **44**, 297-305 (1957).
4. A. W. Sylvester, W. Z. Cande, M. Freeling, Division and differentiation during normal and *liguleless-1* maize leaf development. *Development* **110**, 985–1000 (1990).
5. J. W. Satterlee, M. J. Scanlon, Coordination of leaf development across developmental axes. *Plants* **8**, 433 (2019).
6. K. Esau, Plant Anatomy. *John Wiley and Sons* (1965).
7. J. A. Langdale, B. Lane, M. Freeling, T. Nelson, Cell lineage analysis of maize bundle sheath and mesophyll cells. *Dev Biol* **133**, 128–139 (1989).
8. S. H. Russell, R. F. Evert, Leaf vasculature in Zea mays L. *Planta* **164**, 448–458 (1985).
9. T. Nelson, N. Dengler, Leaf vascular pattern formation. *Plant Cell* **9**, 1121–1122 (1997).
10. B. C. Sharman, Developmental anatomy of the shoot of Zea mays L. *Ann Bot* **6**, 245–282 (1942).
11. E. Scarpella, D. Marcos, J. Friml, T. Berleth, Control of leaf vascular patterning by polar auxin transport. *Genes Dev* **20**, 1015 (2006).
12. K. Bainbridge, *et al.*, Auxin influx carriers stabilize phyllotactic patterning. *Genes Dev* **22**, 810–823 (2008).
13. D. Reinhardt, *et al.*, Regulation of phyllotaxis by polar auxin transport. *Nature* **426**, 255–260 (2003).
14. E. Benková, *et al.*, Local, efflux-dependent auxin gradients as a common module for plant organ formation. *Cell* **115**, 591–602 (2003).
15. M. Biedroń, A. Banasiak, Auxin-mediated regulation of vascular patterning in *Arabidopsis* thaliana leaves. *Plant Cell Reports* **37**, 1215–1229 (2018).
16. N. M. Linh, C. Verna, E. Scarpella, Coordination of cell polarity and the patterning of leaf vein networks. *Curr Opin Plant Biol* **41**, 116–124 (2018).
17. M. S. Matthes, *et al.*, Auxin EvoDevo: conservation and diversification of genes regulating auxin biosynthesis, transport, and signaling. *Mol Plant* **12**, 298–320 (2019).
18. W. Y. Liu, *et al.*, Regulators of early maize leaf development inferred from transcriptomes of laser capture microdissection (LCM)-isolated embryonic leaf cells. *Proc Natl Acad Sci* **119**, e2208795119 (2022).
19. W. Y. Liu, *et al.*, Maize ANT1 modulates vascular development, chloroplast development, photosynthesis, and plant growth. *Proc Natl Acad Sci* **117**, 21747–21756 (2020).
20. T. E. Hughes, O. V. Sedelnikova, H. Wu, P. W. Becraft, J. A. Langdale, Redundant SCARECROW genes pattern distinct cell layers in roots and leaves of maize. *Development* **146**, dev177543 (2019).
21. T. E. Hughes, O. Sedelnikova, M. Thomas, J. A. Langdale, Mutations in NAKED-ENDOSPERM IDD genes reveal functional interactions with SCARECROW during leaf patterning in C4 grasses. *PLoS Genet* **19**, e1010715 (2023).
22. Q. Liu, *et al.*, SHORT ROOT and INDETERMINATE DOMAIN family members govern PIN-FORMED expression to regulate minor vein differentiation in rice. *Plant Cell* **35**, 2848–2870 (2023).
23. T. L. Slewinski, *et al.*, Short-Root1 plays a role in the development of vascular tissue and Kranz anatomy in maize leaves. *Mol Plant* **7**, 1388-1392 (2014).
24. M. L. Schuler, O. V. Sedelnikova, B. J. Walker, P. Westhoff, J. A. Langdale, SHORTROOT-Mediated increase in stomatal density has no impact on photosynthetic efficiency. *Plant Physiol* **176**, 757–772 (2018).
25. D. Vlad, *et al.*, The WIP6 transcription factor TOO MANY LATERALS specifies vein type in C4 and C3 grass leaves. *bioRxiv* 2023.12.20.572592 (2023).
26. J. M. Robil, P. McSteen, Hormonal control of medial–lateral growth and vein formation in the maize leaf. *New Phytologist* **238**, 125–141 (2023).
27. I. R. A. Smillie, K. A. Pyke, E. H. Murchie, Variation in vein density and mesophyll cell architecture in a rice deletion mutant population. *J Exp Bot* **63**, 4563–4570 (2012).

28. S. Leiboff, *et al.*, Genetic control of morphometric diversity in the maize shoot apical meristem. *Nature Communications 2015* **6**, 1–10 (2015).
29. P. Glenn, *et al.*, Wheat bZIPC1 interacts with FT2 and contributes to the regulation of spikelet number per spike. *Theoretical and Applied Genetics* **136**, 1–20 (2023).
30. T. Nobori, M. Oliva, R. Lister, J. R. Ecker, Multiplexed single-cell 3D spatial gene expression analysis in plant tissue using PHYTOMap. *Nature Plants 2023* **9**, 1026–1033 (2023).
31. X. Yang, *et al.*, Spatial transcriptomics of a lycophyte root sheds light on root evolution. *Current Biology* **33**, 4069-4084.e8 (2023).
32. R. Laureyns, *et al.*, An in situ sequencing approach maps PLASTOCHRON1 at the boundary between indeterminate and determinate cells. *Plant Physiol* **188**, 782–794 (2022).
33. M. Pachitariu, C. Stringer, Cellpose 2.0: how to train your own model. *Nature Methods* **19**, 1634–1641 (2022).
34. M. Kitagawa, X. Xu, D. Jackson, Trafficking and localization of KNOTTED1 related mRNAs in shoot meristems. *Commun Integr Biol* **15**, 158-163 (2022).
35. L. G. Smith, D. Jackson, S. Hake, Expression of Knotted1 marks shoot meristem formation during maize embryogenesis. *Dev Genet* **16**, 344–348 (1995).
36. D. Jackson, B. Veit, S. Hake, Expression of maize KNOTTED1 related homeobox genes in the shoot apical meristem predicts patterns of morphogenesis in the vegetative shoot. *Development* **120**, 405–413 (1994).
37. C. C. Martinez, D. Koenig, D. H. Chitwood, N. R. Sinha, A sister of PIN1 gene in tomato (*Solanum lycopersicum*) defines leaf and flower organ initiation patterns by maintaining epidermal auxin flux. *Dev Biol* **419**, 85–98 (2016).
38. D. L. O'Connor, *et al.*, A division in PIN-mediated auxin patterning during organ initiation in grasses. *PLoS Comput Biol* **10**, e1003447 (2014).
39. R. S. Poethig, Clonal analysis of cell lineage patterns in plant development. *Am J Bot* **74**, 581-594 (1987).
40. M. J. Scanlon, K. D. Chen, C. C. McKnight IV, The narrow sheath duplicate genes: sectors of dual aneuploidy reveal ancestrally conserved gene functions during maize leaf development. *Genetics* **155**, 1379–1389 (2000).
41. M. J. Scanlon, M. Freeling, Clonal sectors reveal that a specific meristematic domain is not utilized in the maize mutant narrow sheath. *Dev Biol* **182**, 52–66 (1997).
42. I. Efroni, P. L. Ip, T. Nawy, A. Mello, K. D. Birnbaum, Quantification of cell identity from single-cell gene expression profiles. *Genome Biol* **16**, 1–12 (2015).
43. R. Shahan, *et al.*, A single-cell *Arabidopsis* root atlas reveals developmental trajectories in wild-type and cell identity mutants. *Dev Cell* **57**, 543–560 (2022).
44. C. Kidner, V. Sundaresan, K. Roberts, L. Dolan, Clonal analysis of the *Arabidopsis* root confirms that position, not lineage, determines cell fate. *Planta* **211**, 191–199 (2000).
45. A. E. Richardson, A. Sluis, S. Hake, The Hoja loca1 mutant and AUX/IAA function in phytomer development. *bioRxiv*, 2020.03.27.012211 (2021).
46. J. Strable, *et al.*, Maize YABBY genes drooping leaf1 and drooping leaf2 regulate plant architecture. *Plant Cell* **29**, 1622–1641 (2017).
47. R. Johnston, S. Leiboff, M. J. Scanlon, Ontogeny of the sheathing leaf base in maize (*Zea mays*). *New Phytologist* **205**, 306–315 (2015).
48. Y. Xiong, Y. Jiao, The diverse roles of auxin in regulating leaf development. *Plants* **8** (2019).
49. N. Bhatia, *et al.*, Auxin acts through MONOPTEROS to regulate plant cell polarity and pattern phyllotaxis. *Current Biology* **26**, 3202–3208 (2016).
50. D. Kierzkowski, M. Lenhard, R. Smith, C. Kuhlemeier, Interaction between meristem tissue layers controls phyllotaxis. *Dev Cell* **26**, 616–628 (2013).
51. D. L. O'Connor, *et al.*, Cross-species functional diversity within the PIN auxin efflux protein family. *Elife* **6**, e31804 (2017).

645 **TABLE 1. List of genes used for spatial transcriptomics**
646

| Gene name | Gene_name Maize GDB | Gene ID (v3) | Gene ID (v4) | Gene ID (v5) | Origin of gene name (*supported by phylogeny) | Orthology | Variations |
|---|---|---|---|---|---|---|---|
| *TML1* | dot5 | GRMZMG2150011 | Zm00001d020037_T001 | Zm00001eb309530 | Vlad et al 2024* | AtWIP6 | Previously referred to as Zmdot1 or Zmdot5 |
| *TML2* | – | GRMZM2G134998 | Zm00001d005566_T001 | Zm00001eb097850 | Vlad et al 2024* | AtWIP6 | Previously referred to as Zmdot1h |
| *SCR1* | scro1 | GRMZM2G131516 | Zm00001d052380_T001 | Zm00001eb195650 | Hughes et al. 2019* | AtSCR | |
| *SCR1h* | Gras 37 | GRMZM2G015080 | Zm00001d005029_T001 | Zm00001eb093670 | Hughes et al. 2019* | AtSCR | |
| *SHR1* | Gras 58 | GRMZM2G132794 | Zm00001d029607_T001 | Zm00001eb020840 | Schuler et al. 2017* | AtSHR; OsSHR2 | |
| *SHR2* | Gras 19 | GRMZM2G172657 | Zm00001d021973_T001 | Zm00001eb326020 | Schuler et al. 2017* | AtSHR; OsSHR1 | |
| *SHR2h* | Gras 85 | GRMZM2G019060 | Zm00001d006721_T001 | Zm00001eb108090 | Schuler et al. 2017* | AtSHR; OsSHR1 | |
| *RVN1* | IDD10 | GRMZM2G143723 | Zm00001d039467_T001 | Zm00001eb121010 | Sedelnikova et al. 2018 | – | |
| *RVN1h* | IDD 18 | GRMZM2G046290 | Zm00001d008842_T001 | Zm00001eb337700 | Sedelnikova et al. 2018 | – | |
| *ANT4* | EREB161 | GRMZM2G021573 | Zm00001d048004_T002 | Zm00001eb399440 | Lui et el. 2020* | ANT1-4 all co-orthologs of AtANT1 | |
| *PIN1a* | pin1 | GRMZM2G098643 | Zm00001d044812_T001 | Zm00001eb372180 | Matthes et al. 2019* | Co-ortholog AtPIN1, ortholog | |
| *PIN1d* | pin4 | GRMZM2G171702 | Zm00001d052442_T001 | Zm00001eb196240 | O'Connor et al 2014* | Ortholog of OsPIN1c & OsPIN1d | many papers |
| *LAX1* | aic3 | GRMZM2G149481 | Zm00001d028401_T005 | Zm00001eb010460 | Matthes et al. 2019* | Co-ortholog AtLAX2, OsLAX2 & OsLAX4 | Named ZmLAX2 in Liu et al. 2022 |
| *LAX2* | aic1 | GRMZM2G129413 | Zm00001d030310_T001 | Zm00001eb026490 | Matthes et al. 2019* | Co-ortholog AtLAX2, ortholog of OsLAX4 | |
| *LAX3* | atl1 | GRMZM2G127949 | Zm00001d042809_T003 | Zm00001eb147480 | Matthes et al. 2019* | Co-ortholog AtAUX1 & AtLAX1, ortholog of OsLAX1 | |
| *LAX5* | aic4 | GRMZM2G067022 | Zm00001d038275_T005 | Zm00001eb288800 | Matthes et al. 2019* | Co-ortholog AtAUX1 & AtLAX1, ortholog of OsLAX3 | |
| *HB52* | hb52 | (AC187157.4_FG005) | Zm00001d008869_T001 | Zm00001eb337970 | TAIR | Ortholog of AtHB8 & AtHB15 | |
| *ARF4* | arftf4 | GRMZM2G034840 | Zm00001d001945_T010 | Zm00001eb067270 | Matthes et al. 2019* | Co-ortholog of AtMP, OsARF11 | |
| *ARF29* | arftf29 | GRMZM2G086949 | Zm00001d026540_T016 | Zm00001eb433020 | Matthes et al. 2019* | Co-ortholog of AtMP, OsARF11 | |
| *ARF16* | arftf16 | GRMZM2G028980 | Zm00001d053819_T008 | Zm00001eb207450 | Matthes et al. 2019* | Co-ortholog of AtARF6, ortholog of OsARF6 | |
| *ARF34* | arftf34 | GRMZM2G081158 | Zm00001d031064_T006 | Zm00001eb031700 | Matthes et al. 2019* | Co-ortholog of AtARF6, ortholog of OsARF17 | |
| *ARF23* | arftf23 | GRMZM2G441325 | Zm00001d038698_T007 | Zm00001eb292830 | Matthes et al. 2019* | Co-ortholog of AtARF3 & AtARF4, ortholog of OsARF14 | |
| *KN1* | kn1 | GRMZM2G017087 | Zm00001d033859_T002 | Zm00001eb055920 | Hake et al. 1989 | Class I KNOX | |
| *MYB67* | myb67 | GRMZM2G089244 | Zm00001d053060_T001 | Zm00001eb201150 | Maize GDB | – | |
| *CYC4* | cyc4 | GRMZM2G310115 | Zm00001d012560_T002 | Zm00001eb369340 | Maize GDB | Ortholog of AtCYCB1 genes | |
| *CYC7* | cyc7 | GRMZM2G073003 | Zm00001d043164_T001 | Zm00001eb150450 | Maize GDB | Ortholog of AtCYCB1 genes | previously cyc4b |
| *CYC3* | cyc3 | GRMZM2G073671 | Zm00001d036360_T002 | Zm00001eb272010 | Maize GDB | Ortholog AtCYCB2 genes | |

647

## FIGURE LEGENDS

**Figure. 1: Stages of leaf and vein development in maize shoot apices. A)** Cartoon representation of a longitudinal section across a maize shoot apex. SAM (black) indicates the Shoot Apical Meristem; younger to older stages of leaf development (leaf primordia, P) are indicated using increasing numbers and different colours. The black dotted line indicates the position of the transverse section depicted in (B). **B)** Representative transverse section of a maize shoot stained with Calcofluor and segmented with CellPose. SAM and developing leaf primordia are segmented and colour-coded as in (A). **C)** Vein ranks appear sequentially during leaf primordium development. P1: midvein only (M, cyan); P2: midvein and laterals (L, yellow); P3, P4 and P5: midvein, laterals and intermediate veins (i, magenta). Scale bars = 100 µm.

**Figure 2: *PIN1d* and *LAX5* transcripts mark the P0 primordium. A)** Cluster analysis of cells in the SAM and P1 primordium reveals five domains. **B)** Schematic of shoot apex showing the position of transverse sections illustrated in (C) and (D). **C)** The section taken at the base of the P1 primordium (E1D2) shows that the central zone (*KN1*-expressing) cluster localizes between the developing P1 primordium (red) and the peripheral zone (green). **D)** The section taken at the tip of the P1 primordium (S1A1) shows that the peripheral zone cluster (green) surrounds the central zone cluster (yellow), and includes the putative incipient primordium P0 region. Asterisks highlight cells with primordium identity flanking the P0 region. **E-F)** A subset (arrowhead) of cells from the 'peripheral zone' cluster that co-express *PIN1d* (E) and *LAX5* (F) mark the incipient P0 primordium (G, dotted ellipse). Transcript levels and cell labels are reported in Table S1. Scale bar = 30 µm.

**Figure 3: Distinct auxin transporter profiles mark leaf initiation and midvein specification**. **A-C)** Schematics of sections in longitudinal (A) and transverse view (B, C). P0 = P0 primordium, P1 = P1 primordium, SAM = shoot apical meristem, L1 and L2 define the two layers within the shoot apical meristem. **D-F)** Schematic (D) and spatial transcriptomics (E, F) of *KN1*. Transcripts accumulate in the L2 layer of the shoot apical meristem, with very low or no transcript levels detected in the L1 layer or at the site of P0 initiation (dotted region, E). **G-I)** Schematic (G) and spatial transcriptomics (H, I) of *PIN1d*. Transcripts accumulate predominantly in the initiating P0 primordium (P0) but also in the SAM and the developing P1 primordium (H, I). **J-L)** Schematic (J) and spatial transcriptomics (K, L) of *PIN1a*. Transcripts are detected at the site of the developing midvein in P1 (asterisks), in the initiating P0 primordium and in the central zone of the SAM. **M-O)** Schematic (M) and spatial transcriptomics (N, O) of *LAX3*. Transcripts are detected in the peripheral zone of the SAM, including the P0 initiation site, but not in the developing P1 primordium. Lower transcript levels are detected in the P0 primordium (N) than in the rest of the peripheral zone. **P-R)** Schematic (P) and spatial transcriptomics (Q, R) of *LAX5*. Transcripts are only detected in the initiating P0 primordium, primarily in the L1 layer. Scale bars = 20 µm.

686 **Figure 4: A transcript cluster with vascular identity emerges at P2. A)** Cluster analysis and UMAP
687 plot for the P2 leaf primordium reveals five domains. **B)** Representative image of cluster localisation in
688 a P2 primordium, colour-coded to match (A). **C)** The vasculature cluster marks the midvein (arrowhead)
689 and the developing lateral veins (asterisks). White bracket indicates spacing between veins. **D)** Dot-
690 plot summarising transcript levels in each cluster. Average expression refers to the average transcript
691 level in a cluster (cell type), calculated from the scaled data. Percent expressed refers to the percent
692 of cells in a cluster in which transcripts (as indicated on the x-axis) were detected. Note high levels of
693 *SHR1*, *SHR2*, *ANT4*, *PIN1a* and *LAX2* in the vasculature cluster. Scale bars = 50 µm.
694
695 **Figure 5: Intermediate veins cluster separately from lateral veins at P3 and P4. A, B)** Cluster
696 analyses and UMAP plots of P3 (A) and P4 (B) leaf primordia. **C, D)** Dotplots summarising transcript
697 levels for each gene in each cluster at P3 (C) and P4 (D). Average expression refers to the average
698 transcript level for each gene in a cluster (cell type), calculated from the scaled data. Percent expressed
699 refers to the percent of cells in a cluster in which transcripts (as indicated on the x-axis) were detected.
700 **E, F)** Representative image of cluster localisations in a P3 (E) and P4 (F) primordium, colour-coded to
701 match (A, B). **G, H)** Two distinct vein clusters are identified, lateral (orange) and intermediate
702 (magenta), at both P3 (G) and P4 (H). Scale bars = 50 µm.
703
704 **Figure 6: *PIN1a* accumulation precedes the sequential accumulation of *SHR1* and *LAX2***
705 **transcripts in dividing procambial centres**. **A)** Representative image of *PIN1a* transcript
706 accumulation (red pixels) in the SAM and P1 to P5 leaf primordia. Transcripts accumulate in both the
707 leaf sheath and leaf blade, at all stages of vein development and in all vein ranks. White boxes
708 represent the position of enlargements shown in (B-D). **B, C)** *PIN1a* is detected at low levels in the
709 future midvein at P1 (B - m, circled) and at higher levels at P2 (C- m, circled). **D)** *PIN1a* transcripts are
710 detected in all developing veins within the P5 primordium (m, midvein; i, intermediate; L, lateral). **E)**
711 Superimposed images of *PIN1a* (red) and *SHR1* (blue) transcripts reveal that *PIN1a* accumulation
712 precedes that of *SHR1*. Arrowheads in the inset indicate three developing intermediate veins (i1, i2,
713 i3), in order of their initiation across the medio-lateral leaf axis. *SHR1* transcripts are detected in i1 and
714 i2, but not in the more recently developed i3. **F)** Superimposed images of *SHR1* (blue) and *LAX2*
715 (yellow) transcripts reveal that *SHR1* accumulation precedes that of *LAX2*. Arrowheads in the inset
716 indicate the same developing intermediate veins as in (E): *LAX2* transcripts are not detected in any of
717 these veins but are found in neighbouring older veins. Scale bars = 100 µm.
718
719 **Figure 7: Differentiation of phloem and xylem is accompanied by polar localization of vascular**
720 **markers. A-E)** Transcripts of vascular markers *HB52* (yellow), *LAX2* (blue) and *PIN1a* (red)
721 accumulate in developed and developing veins in all leaf primordia (A). All markers co-localise in
722 developing mid-(B) and lateral (D) veins, with very little adaxial (ad) or abaxial (ab) separation. In
723 differentiated mid-(C) and lateral (E) veins, transcripts preferentially accumulate on the phloem-side (P,

724 as in the case of *HB52*, yellow), xylem-side (X, as in the case of *PIN1a*, red), or juxtaposed (as in the
725 case of *LAX2*, blue). Scale bars = 100 μm (A), 20 μm (B-E).
726

727 **SUPPLEMENTARY FIGURE LEGENDS**

728 **Figure S1 Validation of spatial transcriptomics methodology for localization of transcripts in**
729 **maize shoot apices**. **A)** *KN1* transcripts localize in the shoot apical meristem, specifically the L2 layer
730 as previously shown by in situ hybridization (36). **B)** *PIN1a* transcripts mark all developing veins at all
731 stages of leaf development. **C)** *TML1* transcripts are detected in developing intermediate veins. **D, E)**
732 Molecular cartography (D) and in situ hybridization (E) of *LAX2*. In both cases, transcripts are detected
733 in developing vascular tissue with higher levels detected in major veins (inset, arrowhead) compared
734 to minor veins (inset, asterisks). **F)** *In situ* hybridization control with sense *LAX2* probe. Scale bars =
735 50 µm.

736

737 **Figure S2: Visual representation of clusters at all stages of leaf development.** Sample numbers
738 are depicted across the top and plastochron stages at the left. Cluster colours are as depicted in the
739 main figures. Scale bars = 30 µm (A-F), 50 µm (G-R), 100 µm (S-X).

740

741

742 **Figure S3: Correlation analysis of the Molecular Cartography datasets**. **A)** Correlation plot for
743 comparison of different experimental datasets with the same tissue preparation method. **B)** Correlation
744 plot for comparison of datasets with manual (dataset 3) and automatic (dataset 2) tissue preparation
745 method within the same experiment. **C)** All datasets together. Brown colour indicates negative
746 correlations between rows and columns, blue indicates a positive correlation. The number in each cell
747 represents the correlation coefficient (confidence level = 0.95).

748

749

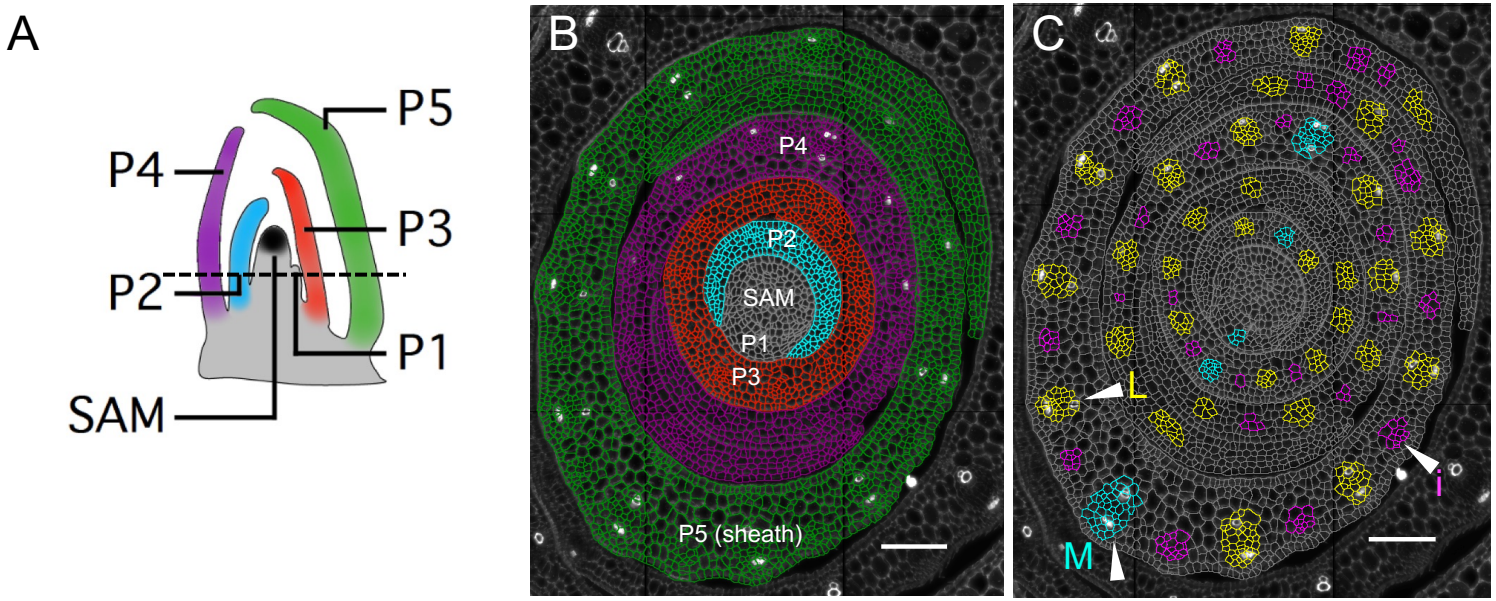


**Figure. 1: Stages of leaf and vein development in maize shoot apices. A)** Cartoon representation of a longitudinal section across a maize shoot apex. SAM (black) indicates the Shoot Apical Meristem; younger to older stages of leaf development (leaf primordia, P) are indicated using increasing numbers and different colours. The black dotted line indicates the position of the transverse section depicted in (B). **B)** Representative transverse section of a maize shoot stained with Calcofluor and segmented with CellPose. SAM and developing leaf primordia are segmented and colour-coded as in (A). **C)** Vein ranks appear sequentially during leaf primordium development. P1: midvein only (M, cyan); P2: midvein and laterals (L, yellow); P3, P4 and P5: midvein, laterals and intermediate veins (i, magenta). Scale bars = 100 µm.

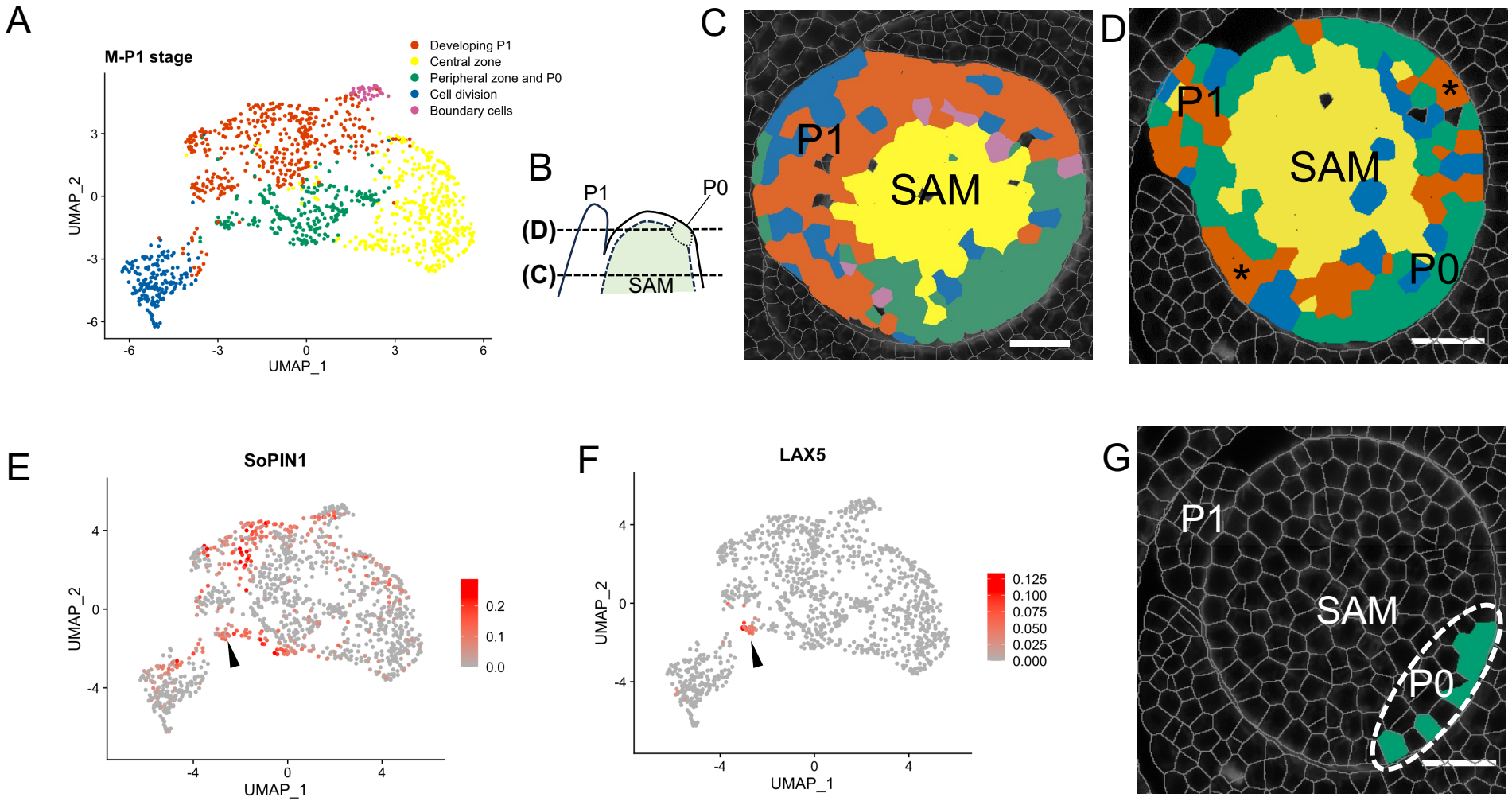


**Figure 2: *PIN1d* and *LAX5* transcripts mark the P0 primordium. A)** Cluster analysis of cells in the SAM and P1 primordium reveals five domains. **B)** Schematic of shoot apex showing the position of transverse sections illustrated in (C) and (D). **C)** The section taken at the base of the P1 primordium (E1D2) shows that the central zone (*KN1*-expressing) cluster localizes between the developing P1 primordium (red) and the peripheral zone (green). **D)** The section taken at the tip of the P1 primordium (S1A1) shows that the peripheral zone cluster (green) surrounds the central zone cluster (yellow) and includes the putative incipient primordium P0 region. Asterisks highlight cells with primordium identity flanking the P0 region. **E-F)** A subset (arrowhead) of cells from the 'peripheral zone' cluster that co-express *PIN1d* (E) and *LAX5* (F) mark the incipient P0 primordium (G, dotted ellipse). Transcript levels and cell labels are reported in Table S1. Scale bar = 30 µm.

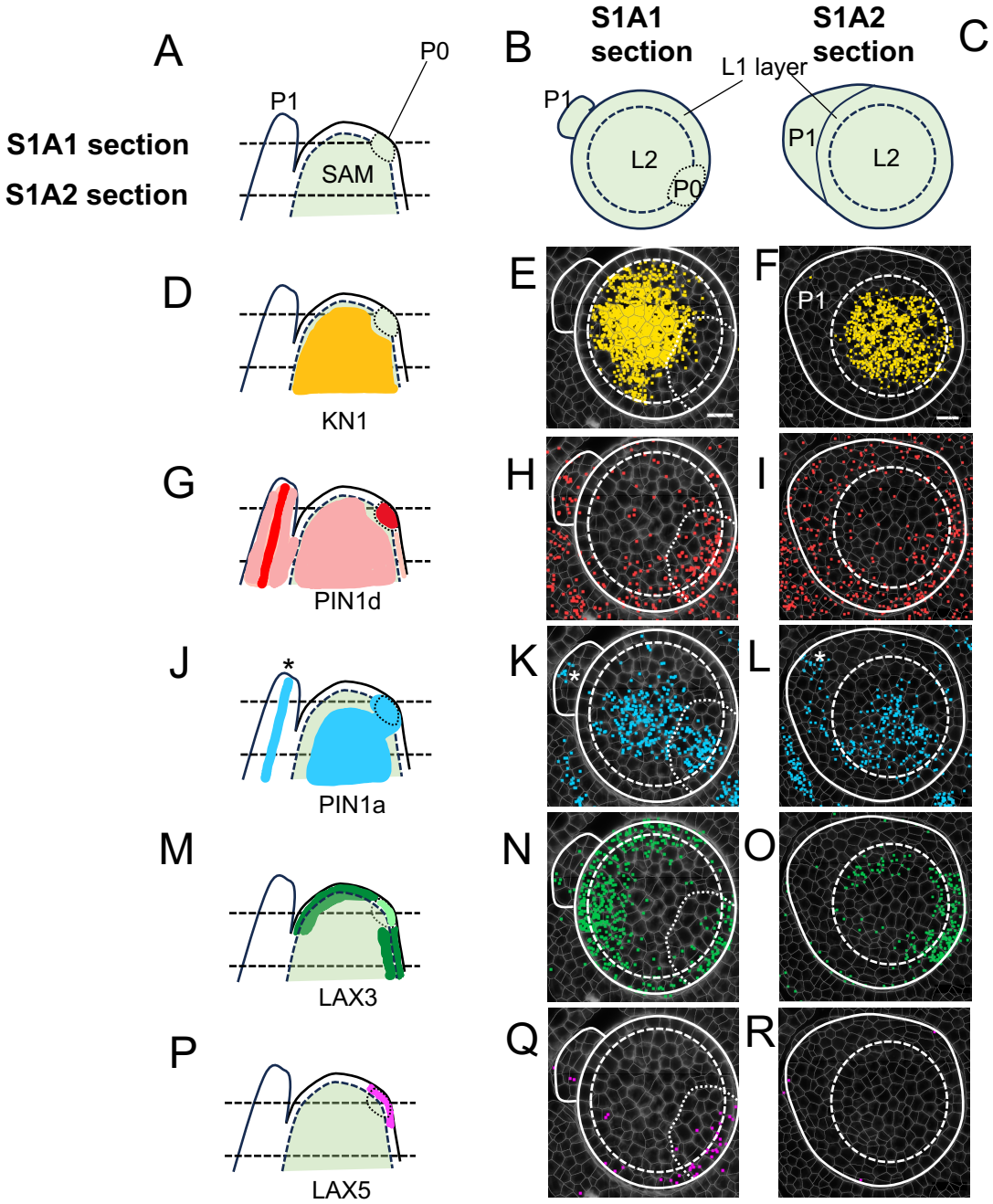


**Figure 3: Distinct auxin transporter profiles mark leaf initiation and midvein specification**. **A-C)** Schematics of sections in longitudinal (A) and transverse view (B, C). P0 = P0 primordium, P1 = P1 primordium, SAM = shoot apical meristem, L1 and L2 define the two layers within the shoot apical meristem. **D-F)** Schematic (D) and spatial transcriptomics (E, F) of *KN1*. Transcripts accumulate in the L2 layer of the shoot apical meristem, with very low or no transcript levels detected in the L1 layer or at the site of P0 initiation (dotted region, E). **G-I)** Schematic (G) and spatial transcriptomics (H, I) of *PIN1d*. Transcripts accumulate predominantly in the initiating P0 primordium (P0) but also in the SAM and the developing P1 primordium (H, I). **J-L)** Schematic (J) and spatial transcriptomics (K, L) of *PIN1a*. Transcripts are detected at the site of the developing midvein in P1 (asterisks), in the initiating P0 primordium and in the central zone of the SAM. **M-O)** Schematic (M) and spatial transcriptomics (N, O) of *LAX3*. Transcripts are detected in the peripheral zone of the SAM, including the P0 initiation site, but not in the developing P1 primordium. Lower transcript levels are detected in the P0 primordium (N) than in the rest of the peripheral zone. **P-R)** Schematic (P) and spatial transcriptomics (Q, R) of *LAX5*. Transcripts are only detected in the initiating P0 primordium, primarily in the L1 layer. Scale bars = 20 µm.

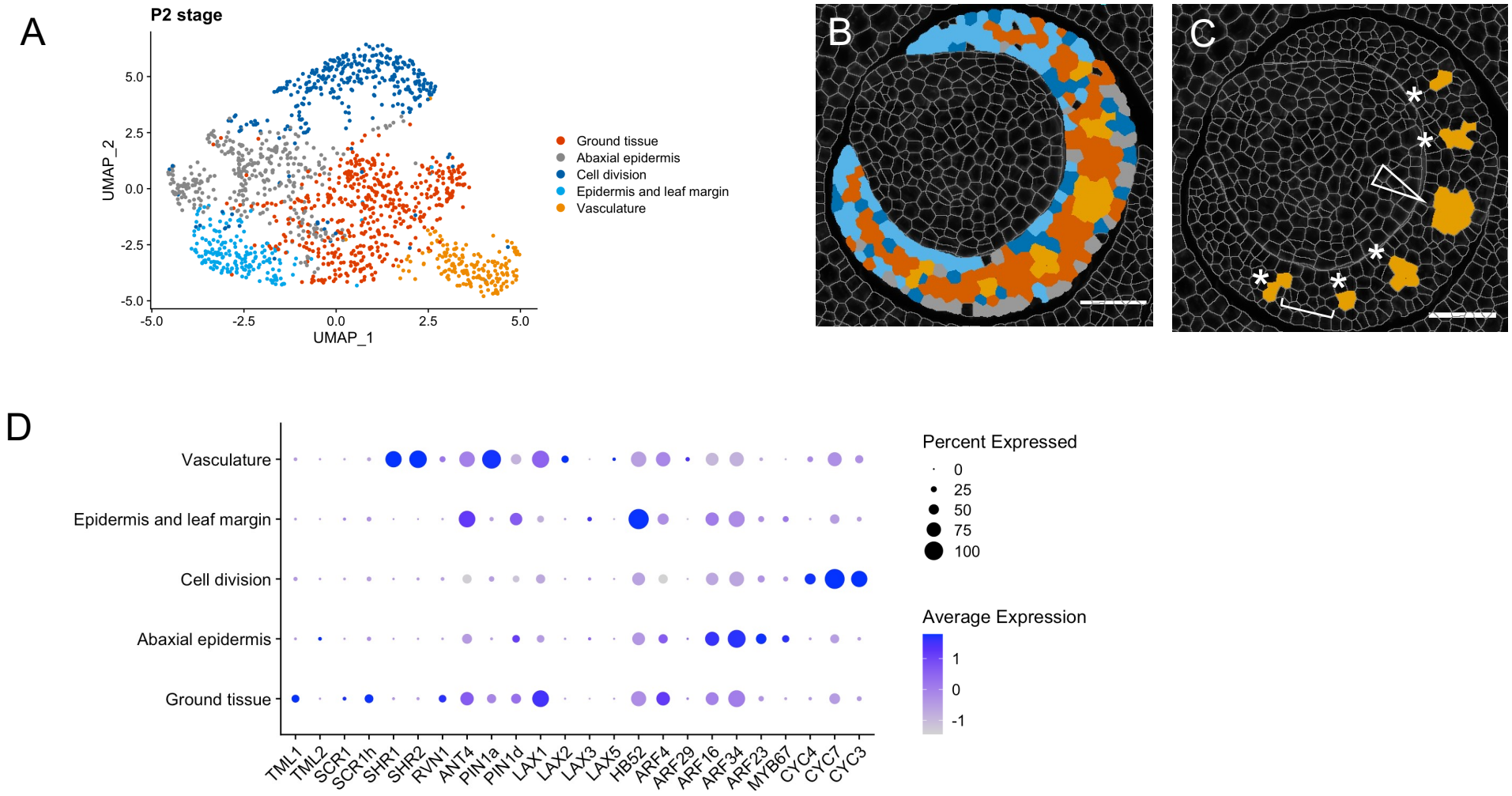


**Figure 4: A transcript cluster with vascular identity emerges at P2. A)** Cluster analysis and UMAP plot for the P2 leaf primordium reveals five domains. **B)** Representative image of cluster localisation in a P2 primordium, colour-coded to match (A). **C)** The vasculature cluster marks the midvein (arrowhead) and the developing lateral veins (asterisks). White bracket indicates spacing between veins. **D)** Dot-plot summarising transcript levels in each cluster. Average expression refers to the average transcript level in a cluster (cell type), calculated from the scaled data. Percent expressed refers to the percent of cells in a cluster in which transcripts (as indicated on the x-axis) were detected. Note high levels of *SHR1*, *SHR2*, *ANT4*, *PIN1a* and *LAX2* in the vasculature cluster. Scale bars = 50 µm.

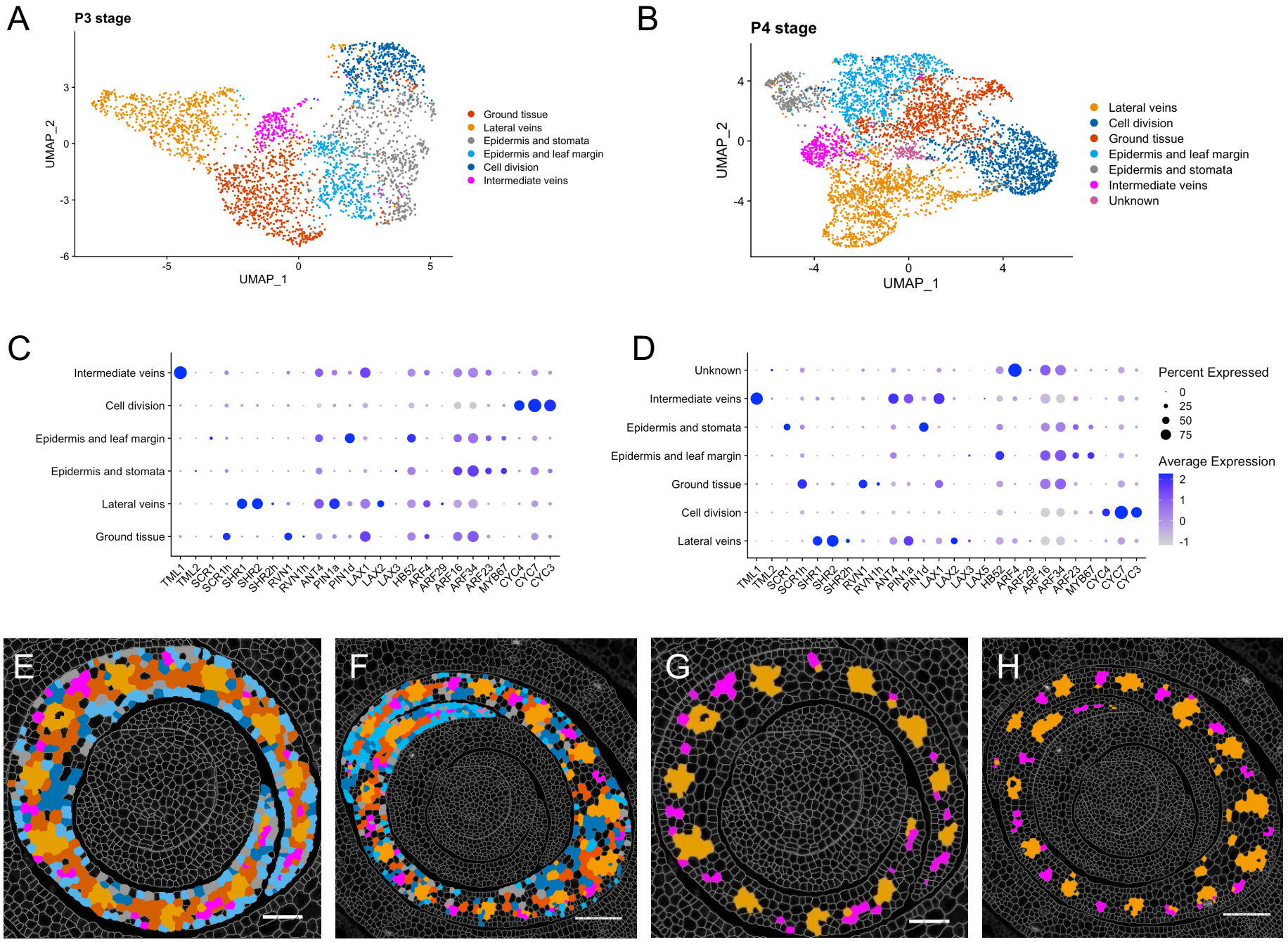


**Figure 5: Intermediate veins cluster separately from lateral veins at P3 and P4. A, B)** Cluster analyses and UMAP plots of P3 (A) and P4 (B) leaf primordia. **C, D)** Dotplots summarising transcript levels for each gene in each cluster at P3 (C) and P4 (D). Average expression refers to the average transcript level for each gene in a cluster (cell type), calculated from the scaled data. Percent expressed refers to the percent of cells in a cluster in which transcripts (as indicated on the x-axis) were detected. **E, F)** Representative image of cluster localisations in a P3 (E) and P4 (F) primordium, colour-coded to match (A, B). **G, H)** Two distinct vein clusters are identified, lateral (orange) and intermediate (magenta), at both P3 (G) and P4 (H). Scale bars = 50 µm.

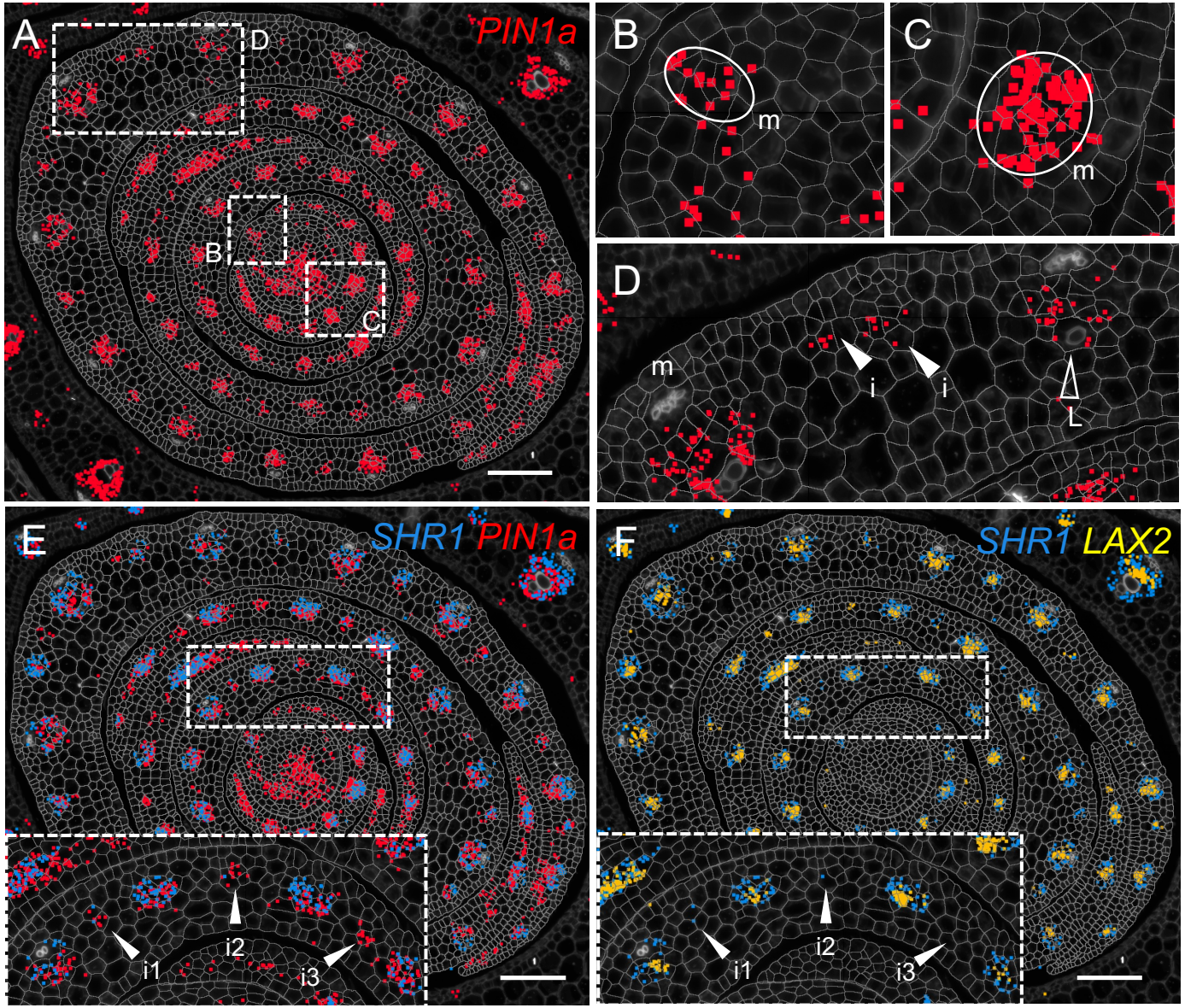


**Figure 6: *PIN1a* accumulation precedes the sequential accumulation of *SHR1* and *LAX2* transcripts in dividing procambial centres**. **A)** Representative image of *PIN1a* transcript accumulation (red pixels) in the SAM and P1 to P5 leaf primordia. Transcripts accumulate in both the leaf sheath and leaf blade, at all stages of vein development and in all vein ranks. White boxes represent the position of enlargements shown in (B-D). **B, C)** *PIN1a* is detected at low levels in the future midvein at P1 (B - m, circled) and at higher levels at P2 (C- m, circled). **D)** *PIN1a* transcripts are detected in all developing veins within the P5 primordium (m, midvein; i, intermediate; L, lateral). **E)** Superimposed images of *PIN1a* (red) and *SHR1* (blue) transcripts reveal that *PIN1a* accumulation precedes that of *SHR1*. Arrowheads in the inset indicate three developing intermediate veins (i1, i2, i3), in order of their initiation across the medio-lateral leaf axis. *SHR1* transcripts are detected in i1 and i2, but not in the more recently developed i3. **F)** Superimposed images of *SHR1* (blue) and *LAX2* (yellow) transcripts reveal that *SHR1* accumulation precedes that of *LAX2*. Arrowheads in the inset indicate the same developing intermediate veins as in (E): *LAX2* transcripts are not detected in any of these veins but are found in neighbouring older veins. Scale bars = 100 µm.

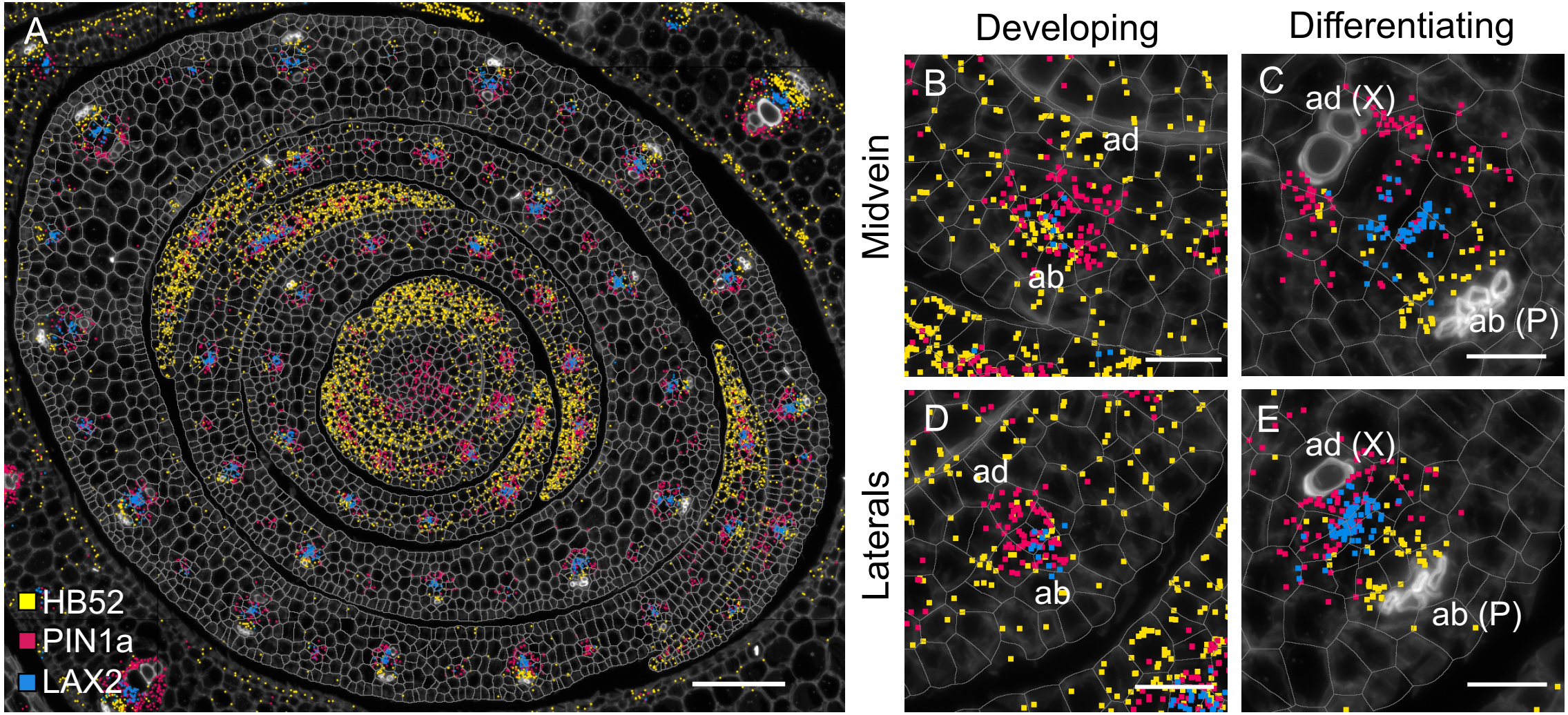


**Figure 7: Differentiation of phloem and xylem is accompanied by polar localization of vascular markers. A-E)** Transcripts of vascular markers *HB52* (yellow), *LAX2* (blue) and *PIN1a* (red) accumulate in developed and developing veins in all leaf primordia (A). All markers co-localise in developing mid-(B) and lateral (D) veins, with very little adaxial (ad) or abaxial (ab) separation. In differentiated mid-(C) and lateral (E) veins, transcripts preferentially accumulate on the phloem-side (P, as in the case of *HB52*, yellow), xylem-side (X, as in the case of *PIN1a*, red), or juxtaposed (as in the case of *LAX2*, blue). Scale bars = 100 µm (A), 20 µm (B-E).

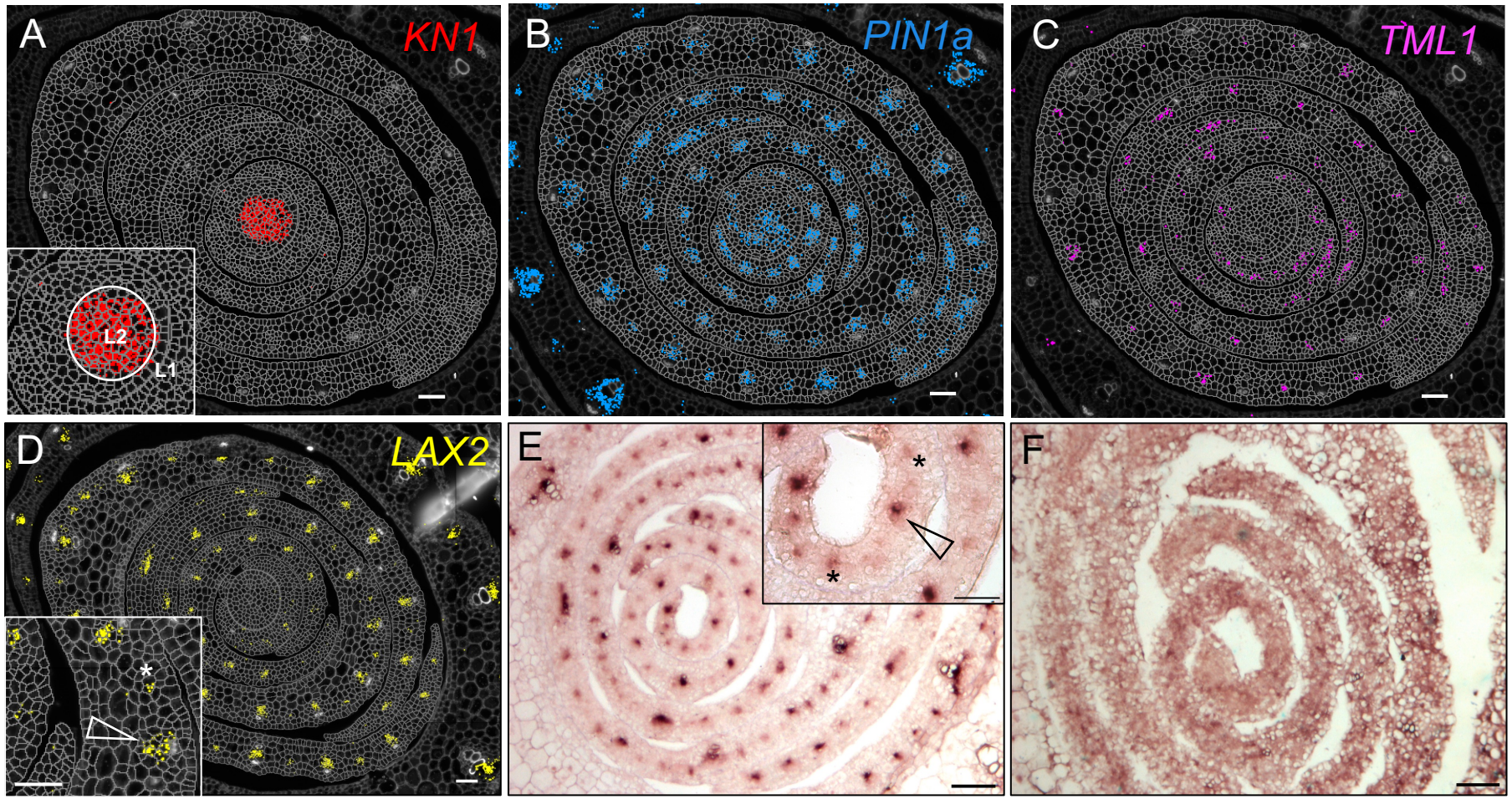


**Figure S1: Validation of spatial transcriptomics methodology for localization of transcripts in maize shoot apices**. **A)** *KN1* transcripts localize in the shoot apical meristem, specifically the L2 layer as previously shown by *in situ* hybridization (Jackson et al., 1994). **B)** *PIN1a* transcripts mark all developing veins at all stages of leaf development. **C)** *TML1* transcripts are detected in developing intermediate veins . **D, E)** Molecular cartography (D) and in situ hybridization (E) of *LAX2*. In both cases, transcripts are detected in developing vascular tissue with higher levels detected in major veins (inset, arrowhead) compared to minor veins (inset, asterisks). **F)** *In situ* hybridization control with sense *LAX2* probe. Scale bars = 50 µm.

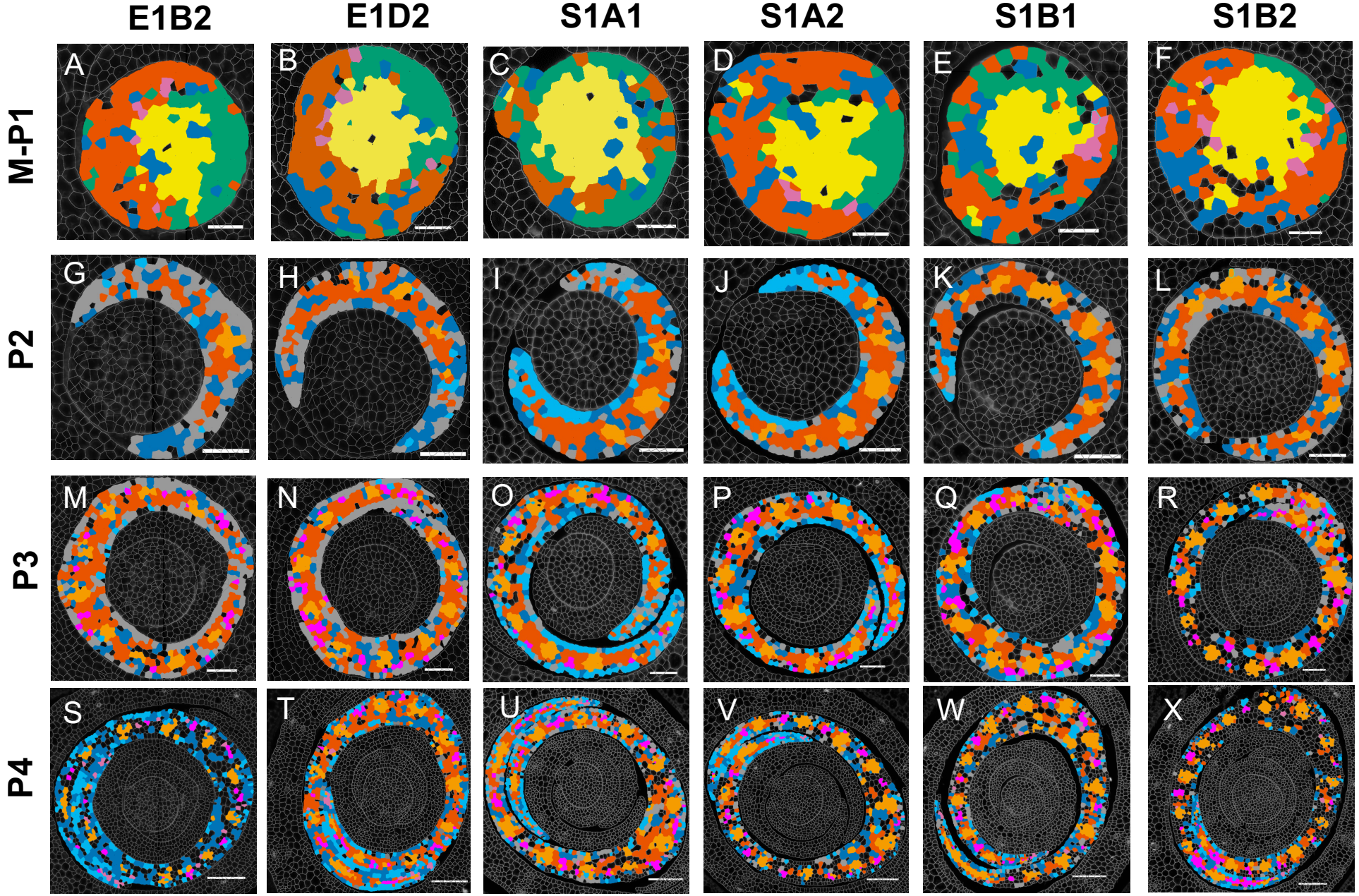


**Figure S2: Visual representation of clusters at all stages of leaf development.** Sample numbers are depicted across the top and plastochron stages at the left. Cluster colours are as depicted in the main figures: A-F refer to the colour scheme in Fig. 2, G-L to the colour scheme in Fig. 4 and M-X to the colour scheme in Fig. 5. Scale bars = 30 µm (A-F), 50 µm (G-R), 100 µm (S-X).

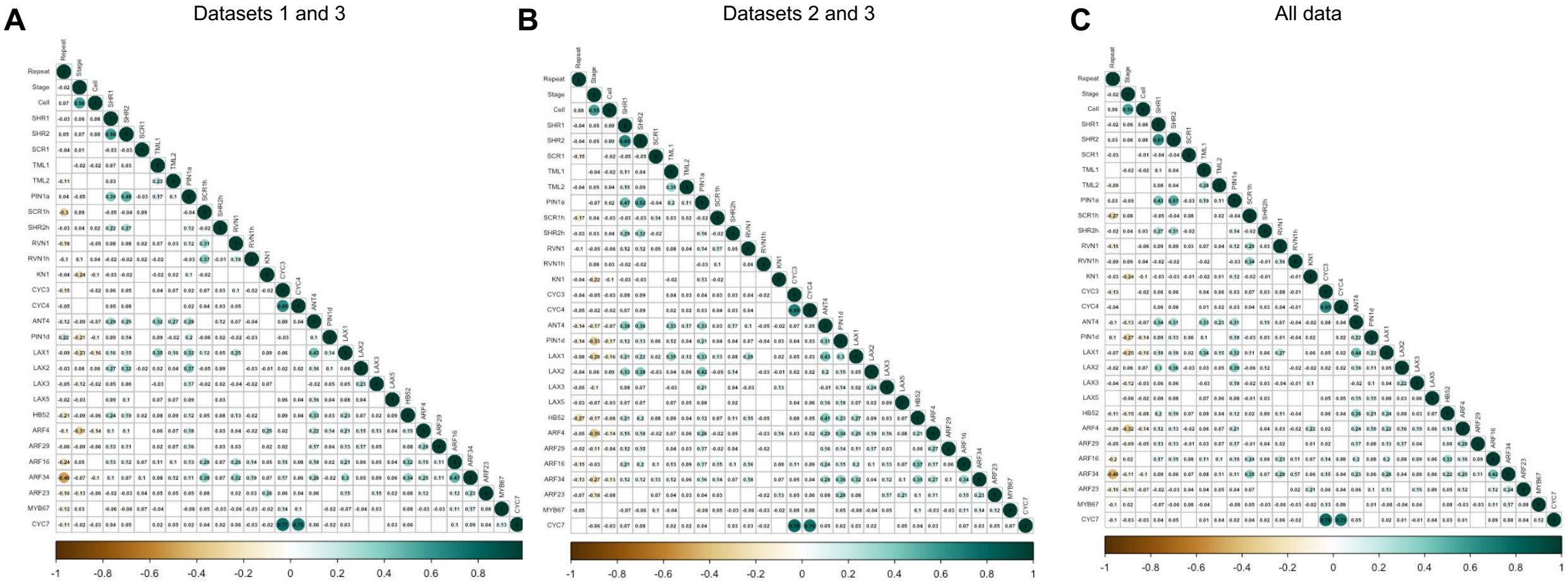


**Figure S3: Correlation analysis of the Molecular Cartography datasets**. **A)** Correlation plot for comparison of different experimental datasets with the same tissue preparation method. **B)** Correlation plot for comparison of datasets with manual (dataset 3) and automatic (dataset 2) tissue preparation method within the same experiment. **C)** All datasets together. Brown colour indicates negative correlations between rows and columns, blue indicates a positive correlation. The number in each cell represents the correlation coefficient (confidence level = 0.95).

| Gene.ID | E1B2_M_P1_23 | E1B2_M_P1_121 | E1B2_M_P1_191 | S1A1_M_P1_39 | S1A1_M_P1_49 | S1A1_M_P1_82 | S1A1_M_P1_83 | **S1A1_M_P1_88** | **S1A1_M_P1_95** | **S1A1_M_P1_100** | **S1A1_M_P1_124** | **S1A1_M_P1_127** | **S1A1_M_P1_150** | S1A1_M_P1_160 | S1A2_M_P1_16 | S1A2_M_P1_72 | S1A2_M_P1_81 | S1A2_M_P1_234 | S1B1_M_P1_183 |
|---|---|---|---|---|---|---|---|---|---|---|---|---|---|---|---|---|---|---|---|
| SHR2 | 0 | 0 | 0 | 0 | 0 | 0 | 0 | 0 | 0 | 0 | 0 | 0 | 0 | 0 | 0 | 0 | 0 | 0 | 0 |
| TML2 | 0 | 0 | 0 | 0 | 0 | 0 | 0 | 0 | 0 | 0 | 0 | 0 | 0 | 0 | 0 | 0 | 0 | 0 | 0 |
| PIN1a | 0 | 0 | 1 | 0 | 0 | 3 | 0 | 1 | 3 | 6 | 0 | 0 | 3 | 0 | 1 | 0 | 0 | 0 | 0 |
| SCR1h | 0 | 0 | 0 | 0 | 1 | 1 | 0 | 0 | 0 | 0 | 0 | 0 | 0 | 0 | 0 | 0 | 0 | 0 | 1 |
| RVN1 | 0 | 0 | 0 | 0 | 0 | 0 | 0 | 0 | 0 | 0 | 0 | 0 | 0 | 0 | 0 | 0 | 0 | 0 | 0 |
| KN1 | 1 | 3 | 0 | 0 | 0 | 14 | 0 | 0 | 0 | 0 | 0 | 0 | 0 | 0 | 0 | 0 | 0 | 0 | 0 |
| CYC3 | 1 | 0 | 0 | 0 | 0 | 0 | 0 | 0 | 1 | 2 | 0 | 1 | 0 | 0 | 0 | 0 | 0 | 0 | 0 |
| CYC4 | 0 | 0 | 0 | 0 | 0 | 0 | 0 | 0 | 0 | 5 | 2 | 0 | 0 | 0 | 0 | 0 | 0 | 0 | 0 |
| ANT4 | 0 | 0 | 0 | 2 | 0 | 0 | 3 | 0 | 0 | 5 | 1 | 0 | 4 | 6 | 0 | 0 | 2 | 0 | 0 |
| PIN1d | 0 | 0 | 0 | 0 | 2 | 0 | 7 | 6 | 5 | 16 | 2 | 3 | 10 | 4 | 0 | 2 | 1 | 3 | 1 |
| LAX1 | 0 | 0 | 0 | 0 | 0 | 0 | 0 | 1 | 0 | 1 | 0 | 2 | 0 | 0 | 0 | 0 | 1 | 0 | 1 |
| LAX3 | 0 | 0 | 1 | 1 | 0 | 8 | 2 | 7 | 1 | 9 | 2 | 3 | 8 | 0 | 0 | 1 | 2 | 2 | 0 |
| LAX5 | 1 | 1 | 1 | 1 | 0 | 2 | 1 | 2 | 2 | 5 | 6 | 3 | 5 | 2 | 1 | 1 | 1 | 1 | 1 |
| HB52 | 0 | 1 | 0 | 0 | 2 | 1 | 0 | 3 | 1 | 5 | 4 | 4 | 2 | 7 | 11 | 4 | 5 | 6 | 0 |
| ARF4 | 1 | 1 | 3 | 0 | 0 | 7 | 4 | 1 | 2 | 0 | 5 | 4 | 0 | 0 | 3 | 1 | 1 | 6 | 0 |
| ARF29 | 1 | 0 | 0 | 0 | 0 | 0 | 0 | 0 | 0 | 0 | 0 | 0 | 0 | 0 | 0 | 0 | 0 | 0 | 0 |
| ARF16 | 0 | 0 | 0 | 0 | 3 | 8 | 2 | 5 | 4 | 2 | 5 | 6 | 1 | 6 | 0 | 0 | 0 | 5 | 1 |
| ARF34 | 5 | 4 | 3 | 2 | 7 | 0 | 1 | 7 | 5 | 9 | 4 | 11 | 7 | 5 | 2 | 6 | 3 | 1 | 5 |
| ARF23 | 0 | 0 | 0 | 0 | 6 | 1 | 3 | 3 | 10 | 21 | 12 | 14 | 13 | 3 | 1 | 0 | 4 | 2 | 1 |
| MYB67 | 0 | 0 | 0 | 0 | 0 | 0 | 0 | 1 | 0 | 0 | 0 | 1 | 1 | 0 | 0 | 0 | 0 | 0 | 0 |
| CYC7 | 1 | 0 | 1 | 1 | 7 | 0 | 0 | 3 | 15 | 21 | 27 | 14 | 2 | 3 | 9 | 0 | 1 | 0 | 0 |

**Table S1: Gene expression in P0 cells identified from the ‘peripheral zone’ cluster.**